



Published in final edited form as:

ACS Nano. 2023 December 26; 17(24): 25157–25174. doi:10.1021/acsnano.3c08088.

Co-Delivery of Bioengineered Exosomes and Oxygen for Treating Critical Limb Ischemia in Diabetic Mice

Ting Zhong,

Department of Mechanical Engineering & Materials Science, McKelvey School of Engineering, Washington University in St. Louis, St. Louis, Missouri 63130, United States

Ning Gao,

Institute of Materials Science and Engineering, McKelvey School of Engineering, Washington University in St. Louis, St. Louis, Missouri 63130, United States

Ya Guan,

Institute of Materials Science and Engineering, McKelvey School of Engineering, Washington University in St. Louis, St. Louis, Missouri 63130, United States

Zhongting Liu,

Institute of Materials Science and Engineering, McKelvey School of Engineering, Washington University in St. Louis, St. Louis, Missouri 63130, United States

Jianjun Guan

Department of Mechanical Engineering & Materials Science, McKelvey School of Engineering, Washington University in St. Louis, St. Louis, Missouri 63130, United States; Institute of Materials Science and Engineering, McKelvey School of Engineering and Department of Biomedical Engineering, McKelvey School of Engineering, Washington University in St. Louis, St. Louis, Missouri 63130, United States

Abstract

Diabetic patients with critical limb ischemia face a high rate of limb amputation. Regeneration of the vasculature and skeletal muscles can salvage diseased limbs. Therapy using stem cell-derived exosomes that contain multiple proangiogenic and promyogenic factors represents a promising strategy. Yet the therapeutic efficacy is not optimal because exosomes alone cannot efficiently rescue and recruit endothelial and skeletal muscle cells and restore their functions under hyperglycemic and ischemic conditions. To address these limitations, we fabricated ischemic-limb-targeting stem cell-derived exosomes and oxygen-releasing nanoparticles and codelivered them in order to recruit endothelial and skeletal muscle cells, improve cell survival under ischemia before vasculature is established, and restore cell morphogenic function under high glucose and

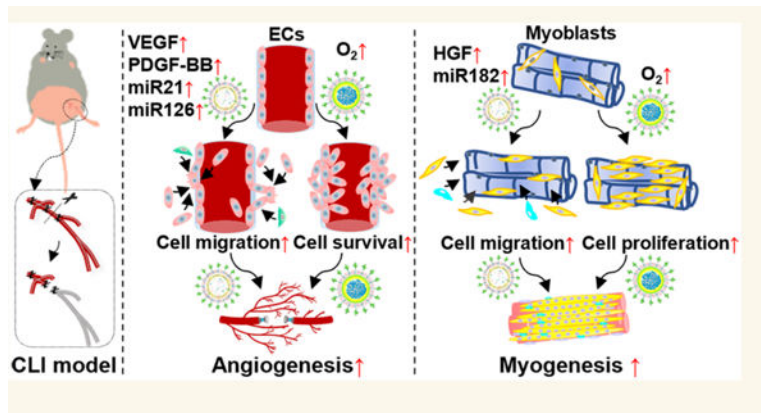
Corresponding Author: Jianjun Guan – *Department of Mechanical Engineering & Materials Science, McKelvey School of Engineering, Washington University in St. Louis, St. Louis, Missouri 63130, United States; Institute of Materials Science and Engineering, McKelvey School of Engineering and Department of Biomedical Engineering, McKelvey School of Engineering, Washington University in St. Louis, St. Louis, Missouri 63130, United States; Phone: 314-935-3537; jguan22@wustl.edu.*
Author Contributions

J.G. and T.Z. designed the study. T.Z., N.G., Y.G., and Z.L. conducted the majority of the experiments. J.G., T.Z., N.G., Y.G., and Z.L. analyzed the results. J.G. and T.Z. wrote the manuscript. J.G. supervised the project.

The authors declare no competing financial interest.

ischemic conditions. The exosomes and oxygen-releasing nanoparticles, delivered by intravenous injection, specifically accumulated in the ischemic limbs. Following 4 weeks of delivery, the exosomes and released oxygen synergistically stimulated angiogenesis and muscle regeneration without inducing substantial inflammation and reactive oxygen species overproduction. Our work demonstrates that codelivery of exosomes and oxygen is a promising treatment solution for saving diabetic ischemic limbs.

Graphical Abstract



Keywords

critical limb ischemia; hypoxia-induced exosomes; oxygen-releasing nanoparticles; ischemic-limb-targeting; angiogenesis; muscle regeneration

INTRODUCTION

Peripheral artery disease (PAD), caused by insufficient blood flow to peripheral tissues, affects approximately 6% of adults worldwide (>230 million), and the prevalence has been climbing.^{1,2} Critical limb ischemia (CLI) is recognized as the most advanced manifestation of PAD.³ The incidence of CLI is reported to be 2- to 7-fold higher in diabetic patients than in the nondiabetic population.⁴ Patients with both diabetes and CLI are at the highest risk for lower-extremity amputations, because mild or major amputation will be performed when invasive treatments cannot be utilized or have proven useless.⁵ Revascularization, either through surgical bypass⁶ or endovascular therapy (EVT),⁷ directly promotes blood flow to the extremities and has been regarded as the first-line therapy for patients with PAD.⁸ However, not all patients are eligible for these procedures, and effective treatments for patients with diabetes and CLI are clearly necessary.

Cell-based therapy has been extensively explored as an attractive alternative for treating patients with no-option CLI.⁹ Autologous bone marrow mononuclear cells (BM-MNCs),¹⁰ bone marrow-derived mesenchymal stem cells (BM-MSCs),¹¹ and CD34⁺ bone marrow cells¹⁰ have been employed as repair cell sources in treating CLI in diabetic patients. Pilot studies have demonstrated that most stem cell therapies can stimulate lower limb ischemic angiogenesis and neovascularization¹² through the paracrine effects, the secretion

of manifold biologically active substances,¹³ leading to increased blood flow to the transplantation area.^{12,14} However, the safety, efficacy, scalability, and reproducibility of stem cell therapy blocks its extensive clinical application.^{15,16} Alternatively, using exosomes that are derived from stem cells and rich in bioactive molecules such as microRNAs (miRNAs) opens new perspectives for cell-free therapy for CLI treatment. Stem cell-derived exosomes can contain miRNAs capable of regulating endothelial and skeletal muscle cell functions, such as miR-21, miR-126, miR-133, miR-182, and miR-206, for not only vascularization but also skeletal muscle regeneration.^{17–23} Notably, exosomes derived from mesenchymal stem cells (MSCs) also contain proangiogenic and promyogenic growth factors, such as vascular endothelial growth factor (VEGF), fibroblast growth factor (FGF), platelet-derived growth factor BB (PDGF-BB), and hepatocyte growth factor (HGF).^{17–23} Using exosomes for CLI treatment is superior to growth factor and miRNA therapies since vascularization and muscle regeneration simultaneously require multiple factors, and these can be provided by exosomes but not readily by delivery systems for growth factors and miRNAs.²⁴

While stem cell-derived exosomes have shown encouraging therapeutic effects for ischemic limbs without diabetes,^{17–23,25–27} the efficacy of current exosome therapy for diabetic ischemic limbs is not most favorable.²⁴ Current exosomes are not tailored with an optimal composition of proangiogenic and promyogenic factors for accelerated vascularization and myogenesis. While exosomes can be engineered to contain exogenous cargos necessary for these processes, current approaches typically use soluble biochemicals and growth factors, which may complicate both the exosome composition as well as the resulting therapeutic effects.^{28–30} Approaches are needed that can upregulate the expression of pro-angiogenic and promyogenic factors in exosomes using insoluble factors.

Furthermore, the hyperglycemic and ischemic conditions of diabetic ischemic limbs greatly hinder exosomes in efficiently rescuing and recruiting endothelial and skeletal muscle cells and restoring their functions, such as migration and morphogenesis.^{31,32} In addition, before exosome-induced vascularization is established, the cells in the limbs, and those recruited to the limbs by exosomes, experience significant death under the extremely low O₂ condition (<1%) of diabetic ischemic limbs.³¹

Here we describe an approach to address the limitations associated with exosome therapy. By codelivering exosomes engineered with upregulated proangiogenic and promyogenic factors and oxygen-releasing nanoparticles, we can synergistically recruit endothelial and skeletal muscle cells, improve their survival under ischemia before vasculature is established, and restore their morphogenic function in promoting vascularization and muscle regeneration. The exosomes and oxygen-releasing nanoparticles can specifically target ischemic limbs after intravenous injection. We observed that the exosomes and oxygen-releasing nanoparticles synergistically improved cell survival, migration, and morphogenesis, facilitating angiogenesis and muscle regeneration.

RESULTS AND DISCUSSION

Upregulating Proangiogenic and Promyogenic Factors in Exosomes Isolated from Induced Pluripotent Stem Cell (iPSC) Derived MSCs (iMSCs), and Endowing These Exosomes with Ischemic-Limb-Targeting Capability.

Hypoxia conditioning was used to modulate the expression of proangiogenic and promyogenic factors (growth factors and miRNAs) in iMSC-derived exosomes (Figure 1A). Using the normoxic condition (21% O₂) for comparison, we evaluated the changes in expression level under induced hypoxia (1% O₂, or 5% O₂). The exosomes exhibited typical exosome markers (Figure 1B), including cluster of differentiation 81 (CD81), intercellular adhesion molecule 1 (ICAM-1), programmed cell death 6 interacting protein (PDCD6IP, also known as ALIX), and Annexin A5 (ANXA5). The exosomes did not show the cell membrane marker GM130. The exosome composition was dependent on the O₂ level. The exosomes from iMSCs cultured under 1% O₂ exhibited significantly higher expressions of proangiogenic PDGF-BB, VEGF, and promyogenic HGF than those from iMSCs cultured under 21% and 5% O₂ (Figure 1C–E). Interestingly, these exosomes also had significantly greater expressions of proangiogenic miR-126 and miR-21, and promyogenic miR-182 (Figure 1F–H).

To increase the circulation time of the exosomes after intravenous (IV) injection and enable the exosomes to target ischemic limbs, they were cloaked with non-prothrombotic platelet membrane that was conjugated with an ischemia-targeting peptide CSTSMLKAC (CST) (Figure 1A).^{33–37} Successful functionalization of the exosomes was confirmed by the transmission electron microscope (TEM) images. Compared to exosomes without functionalization (Figures 1I & S1A), the exosomes functionalized with platelet membrane and CST (ILTEXO) exhibited a unilamellar membrane (Figures 1J & S1B). Confocal images demonstrated that CST was present on the exosomes (Figure 1K). The functionalization increased the diameter of the exosomes from 102.0 ± 3.4 nm (Figure 1L) to 138.6 ± 7.8 nm (Figure 1M). To determine the stability of the functionalized exosomes, they were incubated in 37 °C simulated body fluid. After 28 days, ILTEXO maintained shape and structural integrity (Figure S2A). The size was slightly decreased to 115.8 ± 2.5 nm.

To determine the intracellular uptake of ILTEXO, we used human umbilical vein endothelial cells (HUVECs), mouse myoblast cells (C2C12), and THP-1-derived macrophages (THP-1 derived MØ), representing the major cell types in ischemic limbs. Considering that collagen is a prevalent component of the extracellular matrix in tissues,³⁸ vascular damage during ischemic injuries exposes collagen,³⁹ and platelet membrane selectively binds to collagen,⁴⁰ we opted to use collagen-coated plates to mimic the cellular microenvironment encountered in ischemic sites. After 2 h of incubation with ILTEXO under hypoxia (1% O₂), EXO was found inside 24.7% of the HUVECs, 24.6% of the C2C12 cells, and 36.3% of the THP-1-derived macrophages (Figure 1N, O).

Fabricating Ischemic-Limb-Targeting Oxygen-Releasing Nanoparticles.

We fabricated oxygen-releasing nanoparticles with a core–shell structure (Figure 2A), in which a polyvinylpyrrolidone (PVP)/ hydrogen peroxide (H₂O₂) complex was used

as the core, and the degradable polymer poly(*N*-isopropylacrylamide-*co*-hydroxyethyl methacrylate-*co*-acrylate-oligolactide-*co*-*N*-acryloxysuccinimide) formed the shell. To allow the PVP/H₂O₂ released during shell polymer degradation to be timely converted into molecular oxygen, catalase was conjugated onto the nanoparticle surface (Figure 2A). This design keeps released H₂O₂ from directly contacting with cells after *in vivo* injection. The catalase conjugation was confirmed by confocal images using fluorescein isothiocyanate (FITC) labeled catalase (Figure 2B). The nanoparticles assumed a core-shell structure where a two-layered morphology was observed (Figures 2C & S1C). To provide the nanoparticles with ischemic limb targeting capability, they were extruded with a CST-conjugated platelet membrane, which coated them. The platelet membrane cloaking was evidenced by a trilayered structure in TEM images (Figures 2D & S1D). The resulting ischemic limb targeting, oxygen-releasing nanoparticles (ILTONP) had a hydrodynamic diameter of 170.1 ± 4.6 nm (Figure 2E), greater than that of nanoparticles without platelet membrane cloaking (ONP, 153.8 ± 2.8 nm). The surface ζ potential of ILTONP was -27.0 ± 0.9 mV (Figure 2F), similar to that of the platelet membrane.⁴¹ Additionally, confocal images showed that CST was present on ILTONP (Figure 2G). The ILTONP kept the shape and structural integrity after being incubated in 37 °C simulated body fluid for 28 days (Figure S2B), while the size slightly increased to 180.9 ± 2.6 nm. To determine the oxygen release kinetics of the ILTONP, the nanoparticles were incubated under 1% O₂ that mimicked the oxygen conditions in ischemic limbs. Oxygen was continuously released from the ILTONP for 4 weeks. The oxygen level remained above 10% from day 1 to day 21, and it remained greater than 7% from day 21 to day 28 (Figure 2H). To determine the cellular uptake of ILTONP, we incubated HUVECs, C2C12, and THP-1-derived macrophages with the nanoparticles for 2 h. Confocal images showed that 24.0% of HUVECs, 23.8% of C2C12 cells, and 37.1% of THP-1-derived macrophages were impregnated with ILTONP (Figure 2I, J). These cellular uptake levels were consistent with those of ILTEXO.

Hemocompatibility of Ischemic-Limb-Targeting Exosomes and Oxygen-Releasing Nanoparticles.

Because the ischemic limb-targeting exosomes and oxygen-releasing nanoparticles were designed to be administrated by IV injection, they were tested for hemocompatibility, using a hemolysis assay. After 1 h incubation with the ILTEXO and ILTONP, a low percentage of red blood cells (<10%) had ruptured (Figure 3A). In addition, the extent of hemolysis was similar to that of the blood incubated with phosphate-buffered saline (PBS) (Figure 3B). These results demonstrated that the fabricated ischemic-limb-targeting exosomes and oxygen-releasing nanoparticles had good hemocompatibility.

Ischemic Limb-Targeting Capability of Nanoparticles Cloaked with CST-Conjugated Platelet Membrane Following IV Injection.

To determine whether cloaking with CST-conjugated platelet membrane gave nanoparticles an ischemic limb targeting capability, ILTONP was chosen to be administered via tail IV injection. After 2 days, strong fluorescent signals were observed in the ischemic limbs but not in the contralateral limbs without surgery (Figure 3C), demonstrating preferential enrichment of ILTONP in the ischemic area. It is possible that the ILTONP accumulated in the ischemic limbs through the vasculature bordering the ischemic area and leaky

vasculature in the ischemic area. The ILTONP was not substantially distributed in the major organs, such as liver, spleen, kidneys, heart, and lungs (Figure 3C). The organs in mice injected only with PBS exhibited fluorescence similar to that of the organs in the mice receiving an ILTONP injection. The administration of ILTONP did not increase oxidative stress in these organs as evidenced by reactive oxygen species (ROS) staining (Figure S3). Taken together, the above results demonstrated that the CST-conjugated platelet membrane allowed the nanoparticles to specifically and efficiently target the ischemic limbs, with low off-target distribution and acceptable safety.

Ischemic-Limb-Targeting Exosomes and Oxygen-Releasing Nanoparticles Improved the Survival, Migration, and Morphogenesis of Endothelial Cells and Myoblasts under Ischemia.

In diabetic ischemic limbs, the high glucose and ischemic conditions cause extensive cell death. We evaluated whether ILTONP and ILTEXO had a cytoprotective effect on endothelial cells and myoblasts under these harsh conditions. Two cell types—endothelial cells and myoblasts—are, respectively, responsible for tissue vascularization and muscle regeneration. ILTONP, ILTEXO, and ILTEXO/ILTONP were separately incubated with HUVECs or C2C12 under 1% O₂ in serum-free Dulbecco's Modified Eagle's Medium (DMEM) with 4.5 g/L glucose. After 5 days of incubation, extensive cell death occurred among the HUVECs in the control group, where the double stranded DNA (dsDNA) for live cell content was 5% of that at day 0 (Figure 3D). Treatment with ILTONP or ILTEXO significantly improved HUVEC survival, with the dsDNA content increasing to 43% and 31% of the day 0 values, respectively ($p < 0.0001$ ILTONP vs PBS; $p < 0.0001$ ILTEXO vs PBS). Notably, the combined use of ILTONP and ILTEXO most significantly enhanced HUVEC survival, where the dsDNA content was 70% of the day 0 value ($p < 0.0001$ for ILTEXO/ILTONP vs ILTONP; $p < 0.0001$ for ILTEXO/ILTONP vs ILTEXO). Similar to HUVECs, C2C12 experienced extensive death after 5 days of culture under high glucose and ischemic conditions (Figure 3E). Treating C2C12 with ILTEXO, ILTONP, or ILTEXO/ILTONP significantly promoted cell survival and proliferation: The dsDNA contents were 211%, 987%, and 1189% of the day 0 values, respectively. The above results demonstrated that the oxygen released from ILTONP increased cell survival more than the exosomes in ILTEXO under high glucose and ischemic condition. In addition, ILTONP and ILTEXO exhibited synergistic effects in improving cell survival. To determine whether ILTONP and ILTEXO treatments affected cellular oxidative stress, reactive oxygen species (ROS) staining was conducted on the C2C12 cells. Neither ILTEXO nor ILTONP augmented ROS⁺ cell density under hypoxia (Figure S4).

To determine whether ILTEXO, ILTONP, or ILTEXO/ILTONP could affect the migration of HUVECs and C2C12 under high glucose and ischemic conditions, a two-dimensional (2D) scratch assay was performed. For both cell types, after treatment for 12 and 24 h, the wound areas in the ILTEXO, ILTONP, and ILTEXO/ILTONP groups were significantly decreased compared to the PBS group (Figure 3F–I), suggesting that ILTEXO and ILTONP promoted migration of HUVECs (Figure 3F, G) and C2C12 (Figure 3H, I). The fastest migration was observed for the ILTEXO/ILTONP group, where the wound area was completely closed after 24 h.

We further evaluated whether ILTEXO, ILTONP, or ILTEXO/ILTONP could stimulate the morphogenesis of HUVECs and C2C12 under high glucose and ischemic conditions. The tube formation of HUVECs was analyzed on a 2D collagen gel (Figure 3J, K). HUVECs rarely formed tubular structures on the collagen gel, while coculture with either ILTEXO, ILTONP, or ILTEXO/ILTONP induced significant tube formation ($p < 0.001$ ILTEXO, ILTONP, and ILTEXO/ILTONP vs PBS). These results demonstrate that ILTEXO and ILTONP stimulated endothelial morphogenesis. Comparing the three treatment groups, the number of lumens formed in the ILTEXO/ILTONP group was 2-fold that of the ILTONP group and 3-fold that of the ILTEXO group. Myoblasts are able to differentiate and fuse into myotubes. We found that ILTEXO, ILTONP, and ILTEXO/ILTONP promoted C2C12 to form myotubes under high glucose and ischemic conditions (Figure 3L, M). The density of myotubes with >5 nuclei in the three groups was significantly higher than in the control PBS group ($p < 0.01$ ILTEXO, ILTONP, and ILTEXO/ILTONP vs PBS). Notably, treatment with ILTEXO/ILTONP most significantly stimulated C2C12 to form myotubes, where the myotube density was more than 3 times that in the ILTEXO and ILTONP groups. These results demonstrate that ILTEXO and ILTONP can synergistically facilitate endothelial and myoblast morphogenesis under high glucose and ischemic conditions.

To elucidate the underlying mechanisms by which ILTEXO and ILTONP promoted cell survival, migration, and morphogenesis under high glucose and ischemic conditions, we performed a Western blot analysis of C2C12. The MAPK/Erk1/2 and PI3K/AKT signaling pathways have been shown to be major regulators for cell survival, migration, and morphogenesis.⁴²⁻⁴⁴ We observed that the phosphorylation of Erk1/2 and Akt was more pronounced for cells treated with ILTEXO, ILTONP, or both (Figure 3N-P). Interestingly, ILTEXO more significantly upregulated pAkt expression than ILTONP, and ILTONP mainly upregulated pErk1/2 expression. These results demonstrate that ILTEXO and ILTONP can differentially activate the MAPK/Erk1/2 and PI3K/AKT signaling pathways to improve cell survival, migration, and morphogenesis.

Both Ischemic-Limb-Targeting Exosomes and Oxygen-Releasing Nanoparticles Promoted Cell Survival, Proliferation, and Mitochondrial Metabolism in a Diabetic CLI Model.

A diabetic murine CLI model, in which ischemia was induced by unilateral femoral artery ligation in the hindlimbs of db/db mice (Figure 4A), was used to evaluate the therapeutic efficacy of ILTEXO and ILTONP in ischemic tissues. Five groups of mice, with six mice in each group each, received one of five treatments via tail vein injection: PBS, empty nanoparticles (NP), ILTEXO, ILTONP, or ILTEXO/ILTONP. To determine whether ILTEXO and ILTONP affected cell apoptosis in the ischemic muscles, terminal deoxynucleotidyl transferase dUTP nick end labeling (TUNEL) analysis was performed at 4 weeks after CLI surgery (Figure 4B, E). Notable cell apoptosis was detected in the PBS and NP groups, while cell apoptosis was significantly decreased in the mice treated with ILTEXO or ILTONP ($p < 0.05$ for both ILTEXO or ILTONP vs PBS and ILTEXO or ILTONP vs NP). The cell apoptosis was further significantly decreased in mice receiving the ILTEXO/ILTONP treatment ($p < 0.01$, ILTEXO/ILTONP vs ILTEXO). The exosomes and released oxygen also promoted cell proliferation in the ischemic area. The densities of Ki67⁺ proliferating cells in the groups treated with ILTEXO, ILTONP, and ILTEXO/ILTONP

were significantly greater than those in the PBS or NP groups (Figure 4C, F). The highest Ki67⁺ cell density was observed in the ILTEXO/ILTONP group. These results demonstrate that exosomes and released oxygen synergistically protected cells from high-glucose- and ischemia-induced death and promoted their proliferation.

To determine whether the improved cell survival and proliferation caused by exosomes and released oxygen were due to elevated mitochondrial biogenesis, we evaluated the expression of the transcription coactivator peroxisome proliferator-activated receptor gamma coactivator 1-alpha (PGC-1 α) in the ischemic limbs. Consistent with cell survival and proliferation results, the ILTEXO/ILTONP groups demonstrated a significantly higher PGC-1 α expression than the ILTEXO and ILTONP groups (Figure 4D, G), suggesting that ILTEXO together with ILTONP was conducive to the enhancement of mitochondrial metabolism.

Ischemic-Limb-Targeting Exosomes and Oxygen-Releasing Nanoparticles Promoted Tissue Angiogenesis in a Diabetic CLI Model.

To determine the efficacy of exosomes and released oxygen in stimulating angiogenesis in diabetic ischemic limbs, we monitored their blood perfusion and measured their vessel density. The blood perfusion in the PBS and NP groups increased slowly, with <40% of recovery by day 28 (Figure 5A, B). The ILTEXO and ILTONP treatments significantly improved the blood perfusion compared to the PBS and NP groups, reaching 70% and 74% by day 28, respectively ($p < 0.001$, ILTEXO or ILTONP vs PBS and NP). Notably, in mice receiving the ILTEXO/ILTONP treatment, the blood perfusion in the ischemic hindlimbs was almost completely restored by day 28.

Consistent with the blood perfusion results, sparse isolectin⁺ blood vessels were detected in the PBS and NP groups (Figure 5C). In contrast, abundant isolectin⁺ blood vessels were identified in the ischemic limbs after treatment with ILTEXO, ILTONP, or ILTEXO/ILTONP. In addition, vessel density in the ILTEXO/ILTONP group was 1.5-fold and 2.5-fold greater than that of the ILTEXO and ILTONP groups, respectively (Figure 5D, $p < 0.0001$, ILTEXO/ILTONP vs ILTEXO, ILTONP). Notably, the delivered ILTEXO and ILTONP synergistically enhanced vessel maturation. The density of mature vessels in the ischemic limbs with ILTEXO/ILTONP treatment was significantly higher than that of the untreated (3-fold), NP (3-fold), ILTEXO (1.6-fold), and ILTONP (1.8-fold) groups (Figure 5D). Besides increasing their blood vessel density, treating the diabetic ischemic limbs with ILTEXO, ILTONP, or ILTEXO/ILTONP significantly augmented the expressions of VEGFA and bFGF at mRNA levels (Figure 5F, G). All these findings indicated that exosomes and released oxygen were able to promote angiogenesis in the diabetic ischemic limbs.

Ischemic-Limb-Targeting Exosomes and Oxygen-Releasing Nanoparticles Enhanced Skeletal Muscle Regeneration in a Diabetic CLI Model.

To assess skeletal muscle regeneration following treatments with ILTEXO, ILTONP, or ILTEXO/ILTONP, we evaluated the central nucleus density (Figure 6A, E) and muscle fiber diameter (Figure 6B, F) of skeletal muscles harvested at day 28. Compared to the PBS and NP groups, significant increases in the central nucleus density were observed in the mice

injected with ILTEXO, ILTONP, and ILTEXO/ILTONP ($p < 0.05$, ILTEXO or ILTONP vs PBS, ILTEXO or ILTONP vs NP). Additionally, ILTEXO/ILTONP had the largest muscle myofiber diameter ($p < 0.01$, ILTEXO/ILTONP vs PBS, NP, ILTEXO, or ILTONP). These results demonstrate that both ILTEXO and ILTONP accelerated muscle regeneration in the ischemic areas.

Resident satellite cells are involved in skeletal muscle regeneration after activated satellite cells differentiate to form myofibers. To determine whether delivery of ILTEXO or ILTONP activated satellite cells, immunostaining was performed for both MyoD and Pax7 (Figure 6C). MyoD⁺/Pax7⁺ cells were identified as activated satellite cells. Compared to the PBS and NP groups, the ILTEXO and ILTONP groups had significantly higher densities of MyoD⁺/Pax7⁺ cells ($p < 0.0001$, Figure 6G). These results demonstrate that the delivery of exosomes and oxygen synergistically activated resident satellite cells for myogenesis.

Further, to evaluate the roles of ILTEXO and ILTONP in tissue remodeling, PicroSirius red staining was carried out 28 days after surgery and the total collagen content was calculated. The ILTEXO, ILTONP, and ILTEXO/ILTONP groups had significantly lower total collagen contents than the PBS and NP groups (Figure 6D, H). These results demonstrate that the delivered exosomes and oxygen did not induce fibrosis formation while stimulating skeletal muscle regeneration in the ischemic areas.

Ischemic-Limb-Targeting Exosomes and Oxygen-Releasing Nanoparticles Alleviated ROS and Inflammation in a Diabetic CLI Model.

To determine whether injection of ILTEXO and ILTONP affected inflammation in the ischemic area, proinflammatory M1 macrophages (CD68⁺) and pro-reparative M2 macrophages (CD206⁺) in the tissue were characterized. A significant M1 macrophage density decrease was found for ILTEXO/ILTONP ($p < 0.05$, ILTEXO/ILTONP vs PBS or NP) (Figure 7A, D). Interestingly, the density of M2 macrophages was significantly increased following treatment with ILTEXO, ILTONP, or ILTEXO/ILTONP (Figure 7B, E). These results demonstrate that exosomes and oxygen released from the nanoparticles may help relieve the ischemic limb from violent inflammatory responses and promote muscle repair by macrophage polarization.

In ischemic muscles, excessive ROS generation may lead to cell death and inflammatory responses. To assess whether ILTEXO and ILTONP affected the ROS content in the ischemic area, staining for ROS was performed 4 weeks after surgery. Both ILTEXO and ILTONP significantly reduced the ROS levels, in marked contrast to the higher levels of ROS signals in the PBS- and NP-treated groups (Figure 7C, F). Moreover, the lowest ROS expression was detected in the ILTEXO/ILTONP-treated group, suggesting the beneficial interplay of ILTEXO and ILTONP in reducing ROS in the ischemic region.

In diabetic patients, peripheral artery disease has a 2–4 times greater risk of developing into CLI,^{45–49} a disease with a high rate of eventual limb amputation. Because CLI is characterized by extremely low blood perfusion and degenerated skeletal muscle, regenerating the vasculature and skeletal muscle can salvage the limbs. But under the hyperglycemic and ischemic conditions of diabetic CLI, poor survival and inferior

functioning of the endothelial and skeletal muscle cells impair regeneration.^{46–50} While currently there is no effective treatment, therapy using stem cell-derived exosomes that contain multiple proangiogenic and promyogenic factors stands out as a promising strategy.^{17–22,51–59} Yet the therapeutic efficacy is not optimal, because exosomes alone cannot rescue and recruit endothelial and skeletal muscle cells and cannot restore their functions under hyperglycemia and ischemic conditions.^{24,31}

Here, we addressed the above limitations by codelivering ischemic-limb-targeting stem cell-derived exosomes and O₂-releasing nanoparticles (Figure 8). They performed three functions: (1) the exosomes recruited endothelial and skeletal muscle cells, (2) released oxygen promoted survival of the recruited cells and those existing in the diabetic ischemic limbs before vascularization was established, and (3) the exosomes stimulated the morphogenesis of these cells. The exosomes and sustainedly released oxygen exhibited synergistic effects in promoting cell survival, migration, and morphogenesis. Such synergistic effects have not been found before. The synergistic effects led to quicker restoration of blood perfusion than delivery of exosomes only into diabetic ischemic limbs^{58,60} or delivery of stem cells engineered with improved survival into a less harsh model, ischemic limbs without diabetics.⁶¹

In this work, exosomes were derived from iMSCs. The advantages of using iMSCs are that they exhibit greater proliferation potential than MSCs isolated from adult tissues,⁶² and autologous iMSCs can be used to harvest exosomes that will later be applied to the same patient.⁶² Notably, MSC exosomes contain proangiogenic and promyogenic miRNAs and growth factors.^{17–23} We enhanced the expression of proangiogenic and promyogenic factors in iMSC exosomes by hypoxia conditioning under 1% O₂. The expressions of PDGF-BB, VEGF, and HGF rose by ~1.5-fold, 1.5-fold, and 1.3-fold, respectively, compared to those at 21% O₂ (Figure 1C–E). Furthermore, the expressions of proangiogenic miR-126-3p and miR-21-5p, and promyogenic miR-182-5p were 2.0-fold, 1.3-fold, and 2.2-fold greater than those at 21% O₂ (Figure 1F–H). These results suggested that iMSC exosomes harvested at 1% O₂ had greater angiogenic and myogenic potential than those harvested at normoxia. Hypoxia conditioning has been explored to modulate exosome composition in stem cells, but these works found only one or two growth factors or miRNAs were upregulated under hypoxia.^{63,64} In addition, some studies used serum during cell culture, which complicated the composition of exosomes.^{63–66} In this study, we demonstrated that multiple proangiogenic and promyogenic miRNAs and growth factors were significantly upregulated under 1% O₂ without using serum for cell culture.

CLI is characterized by severe and prolonged hypoxia, which causes extensive cell death and impairs angiogenesis.³¹ Oxygenation of the ischemic limb is thus necessary for cell survival and proliferation and angiogenesis. Oxygen-releasing nanoparticles were therefore developed to gradually supply oxygen to the cells. The nanoparticles were able to directly release molecular oxygen because catalase conjugated on the surface converted the released H₂O₂ into oxygen (Figure 2A).^{67,68} This design kept released H₂O₂ from escaping from the nanoparticles and causing toxic effects. Our oxygen generation approach is thus advantageous over those approaches that release H₂O₂ first and then rely on H₂O₂ decomposition to form oxygen.^{69–71}

Our results demonstrated that both exosomes and oxygen-releasing nanoparticles improved endothelial cell and myoblast survival, migration, and morphogenesis under high glucose and ischemic conditions, mimicking those of diabetic ischemic limbs (Figure 3D–M). The two cell types are responsible for angiogenesis and myogenesis, respectively. Notably, the exosomes and oxygen-releasing nanoparticles exhibited synergistic effects (Figure 3D–M). We found that the exosomes and released oxygen stimulated cell survival, migration, and morphogenesis through different mechanisms (Figure 3N–P). The exosomes mainly activated the Akt and Erk1/2 signaling pathways, while the released oxygen mainly activated the Erk1/2 pathway.

To allow the exosomes and oxygen-releasing nanoparticles delivered by IV injection to have prolonged circulation times and specifically target ischemic limbs, they were cloaked with a CST-functionalized platelet membrane. Previous studies have shown that platelet membrane was able to “disguise” cloaked nanoparticles in the circulation.^{41,72} CST is an ischemia-targeting peptide.^{33–37} We found that the CST-conjugated platelet membrane allowed the nanoparticles to predominantly accumulate in the ischemic limbs (Figure 3C), likely through the vasculature bordering the ischemic area and the leaky vessels in the ischemic area. The delivered exosomes and oxygen-releasing nanoparticles performed synergistically to decrease cell apoptosis, to increase cell proliferation and mitochondrial metabolism, and to augment the expressions of angiogenic growth factors (Figures 4B–G & 5F, G). These beneficial effects led to quicker angiogenesis with blood perfusion being completely restored after 28 days in the group with both exosomes and oxygen-releasing nanoparticles (Figure 5A–E). Besides angiogenesis, the exosomes and oxygen-releasing nanoparticles synergistically promoted skeletal muscle regeneration in the diabetic ischemic limbs. The regenerating muscles exhibited significantly larger myofiber diameters and higher densities of central nuclei and activated satellite cells than those in the groups delivered with either exosomes or oxygen-releasing nanoparticles alone (Figure 6A–C, E–G). Notably, the delivery of exosomes and oxygen-releasing nanoparticles did not induce substantial inflammation or oxidative stress (Figure 7A–F).

This work presents an effective approach to angiogenesis and muscle regeneration in diabetic ischemic limbs. Notwithstanding, we acknowledge several limitations in this study. First, the diabetic murine CLI model we used may not completely mimic the scenario of human patients with CLI. To better test the therapeutic efficacy of exosomes and oxygen-releasing nanoparticles, future studies can use large animals, such as swine, whose pathophysiology is more closely related to that of human. Second, the dose–response effects of exosomes and oxygen-releasing nanoparticles were not investigated. It is possible that a higher dosage will lead to a greater therapeutic efficacy. It is also possible that a higher dosage of oxygen-releasing nanoparticles will increase deteriorative oxidative stress in the tissues. Third, this study used a well-established mouse CLI model,^{73–75} where the limb ischemia was induced by ligating at both the proximal and distal portions of the left femoral artery and vein and completely cutting the vessels between the two sutures. The total loss of blood flow between the two sutures quickly develops an ischemic environment. This model may not completely mimic the conditions of CLI in humans. The exosomes and oxygen-releasing nanoparticles were applied 4 h after ischemia induction. At this time point, the ischemia may not have reached its lowest level. In our future studies, we will apply the

exosomes and oxygen-releasing nanoparticles at different times after ischemia induction and investigate how treatment timing affects therapeutic efficacy.

CONCLUSION

In summary, ischemic-limb-targeting stem cell-derived exosomes and oxygen-releasing nanoparticles were able to recruit endothelial and skeletal muscle cells, improve cell survival under ischemia, and restore cell morphogenic function under high glucose and ischemic conditions. The combined effects of exosomes and released oxygen synergistically promoted angiogenesis and muscle regeneration. Co-delivery of exosomes and oxygen emerges as a promising therapeutic approach for the treatment of diabetic ischemic limbs.

EXPERIMENTAL SECTION

All chemicals were purchased from Sigma-Aldrich unless specified otherwise. Tetramethylrhodamine-functionalized CSTSMLKAC-(CST) was synthesized by GenScript Biotech Corporation.

Cell Lines and Culture.

The induced pluripotent stem cell (iPSC)-derived mesenchymal stem cells (iMSCs) were obtained from FUJIFILM Cellular Dynamics, Inc. and were maintained in serum-free maintenance medium mainly containing Iscove's Modified Dulbecco's Medium (IMDM, Gibco), Ham's F-12 medium (Corning), 50 ng/mL bFGF (Peprotech), 50 ng/mL PDGF-BB (Peprotech), 50 μ g/mL ascorbic acid (Sigma-Aldrich), and 1% penicillin/streptomycin (Gibco). The C2C12 myoblast cell line was provided by the ATCC and cultured in Dulbecco's Modified Eagle's Medium (DMEM) containing 10% fetal bovine serum (FBS, Atlanta Biologicals). Human umbilical vein endothelial cells (HUVECs), purchased from Lonza, were kept in endothelial basal medium-2 (EBM-2, Lonza) supplemented with EGM-2 Endothelial SingleQuots Kit (Lonza). The THP-1 cell line was purchased from ATCC and incubated with Roswell Park Memorial Institute (RPMI) 1640 Medium (ATCC) supplemented with 10% FBS and 0.5 mM 2-mercaptoethanol (Gibco). All cells were cultured at 37 °C in a humidified 5% CO₂ atmosphere.

Isolation of Exosomes Derived from iMSCs.

iMSCs, grown to reach ~70% confluence, were rinsed twice with Dulbecco's phosphate-buffered saline (DPBS, Sigma-Aldrich) and then incubated in the iMSCs maintenance medium at 37 °C in a humidified 5% CO₂ atmosphere under normoxia (21% O₂) or hypoxia (5% or 1% O₂) for 3 days. After incubation, the medium was harvested and centrifuged at 2000 \times g for 30 min to remove the cells and debris. Exosome isolation was conducted using a Total Exosome Isolation Reagent (from cell culture media, Invitrogen). The supernatant was mixed with exosome isolation reagent in a ratio of 1:2 and incubated at 4 °C overnight. The pelleted exosomes were obtained via centrifugation at 10,000 \times g for 1 h at 4 °C. The exosomes were then resuspended in DPBS and filtered through 0.22- μ m sterile filters. The concentration of exosomes was determined using a protein assay dye reagent concentrate (Bio-Rad).

Exosome Biomarker Analysis.

The biomarkers on exosomes were analyzed using an Exo-Check Exosome Antibody Array (System Biosciences). 100 μg of exosomes was lysed with 10 \times lysis buffer followed by labeling the lysate with 1 μL of labeling reagent at room temperature for 30 min. After excess labeling reagent was removed with the provided columns, the labeled lysate was mixed with blocking buffer and then incubated with the provided membrane at 4 $^{\circ}\text{C}$ overnight. The membrane was washed with wash buffer and incubated with detection reagent at room temperature for 30 min, before it was incubated with WesternBright ECL HRP substrate (Advansta) and imaged with a ChemiDoc XRS+ Gel Imaging System (Bio-Rad) with Image Lab software.

Analysis of Proangiogenic and Promyogenic Growth Factors and miRNAs in Exosomes.

The growth factors in exosomes, including vascular endothelial growth factor (VEGF), platelet-derived growth factor (PDGF-BB), and hepatocyte growth factor (HGF), were detected with corresponding enzyme-linked immunosorbent assay (ELISA) kits. Briefly, the exosomes were lysed by RIPA buffer (Sigma-Aldrich) and quantified with a protein assay dye reagent concentrate. Then fractions of the lysed exosomes were subjected to ELISA assays using human VEGF165 (PeproTech), PDGF-BB (PeproTech), and HGF (R&D systems) ELISA kits, respectively.

The miRNAs in exosomes were enriched by using a Total Exosome RNA and Protein Isolation Kit (Invitrogen). The exosomes were resuspended in ice cold exosome resuspension buffer and lysed with one volume of 2 \times denaturing solution on ice for 5 min. After being extracted with one volume of acid-phenol/chloroform, the microRNA was purified by eluting it through filter cartridges with wash buffer. Then MystiCq microRNA cDNA synthesis mix (Sigma-Aldrich) was utilized to convert the enriched microRNA to cDNA. The expressions of miR-21-5p, miR-126-3p, and miR-182-5p were analyzed by using MystiCq microRNA SYBR Green qPCR ReadyMix (Sigma-Aldrich; qPCR = quantitative polymerase chain reaction) on a QuantStudio 5 Real-Time PCR Detection System (Applied Biosystems). MystiCq microRNA qPCR universal PCR primer (Sigma-Aldrich), as well as MystiCq microRNA qPCR assay primers (Sigma-Aldrich), including hsa-miR-21-5p, hsa-miR-126-3p, and hsa-miR-182-5p, were used at a final concentration of 300 nM, while RNU6-1 (Sigma-Aldrich) was used as the control. The relative microRNA expression was calculated according to the standard Ct method.

Preparation of Ischemic-Limb-Targeting Exosomes (IL-TEXO).

To obtain ischemic-limb-targeting exosomes, the exosomes were mixed with the CST-functionalized platelet membrane (Scheme S1) at the same protein concentration and then extruded 20 times with a 400 nm membrane by using a mini-extruder (Avanti Polar Lipids). The resulting ILTEXO was observed by using a Zeiss LSM 880 II Airyscan FAST confocal microscope to confirm that CST was on the ILTEXO.

Preparation of Ischemic-Limb-Targeting Oxygen-Releasing Nanoparticles (ILT-ONP).

The oxygen-releasing nanoparticles were fabricated using poly(*N*-isopropylacrylamide-*co*-hydroxyethyl methacrylate-*co*-acrylate-oligolactide-*co*-*N*-acryloxysuccinimide) as shell and

complex of polyvinylpyrrolidone (PVP) and hydrogen peroxide (H_2O_2) as core. The shell polymer was synthesized following a previously established approach.⁷⁶ The PVP/ H_2O_2 complex was formed by dissolving 24.2 mg of PVP (40 kDa, Fisher Scientific) in 0.1 mL of 30% H_2O_2 . The solution was mixed with 1 mL of 4% shell polymer solution in dichloromethane (DCM) and emulsified using an ultrasonicator (Cole-Parmer) for 1 min to generate a primary emulsion. The emulsion was then added into 10 mL of 4% poly(vinyl alcohol) (PVA, M_w 9000–10000, Sigma-Aldrich) solution followed by ultrasonication for 3 min. The obtained double emulsion was added dropwise into 100 mL of DI water and stirred for 2 h at room temperature to remove the DCM. The nanoparticles were collected via centrifugation at $12,000 \times g$ for 15 min and washed with DI water 3 times. The nanoparticles were then subjected to conjugation with catalase. Ten milligrams of nanoparticles was mixed with 8 mg/mL of catalase from bovine liver (2000–5000 units/mg protein, Sigma) solution and stirred at 4 °C for 4 h. The resulting nanoparticles were washed with DPBS 3 times to remove free catalase. To ascertain the conjugation of catalase onto the nanoparticles, catalase was pre-labeled with fluorescein isothiocyanate (FITC). The fluorescent images of the nanoparticles postcatalase conjugation were acquired using a Zeiss LSM 880 II Airyscan FAST confocal microscope.

To impart the nanoparticles with an ischemic-limb-targeting property, a CST-functionalized platelet membrane was cloaked on the nanoparticles by sonicating a mixture of platelet membrane (derived from 2×10^{10} platelets) with 10 mg of nanoparticles at 130 W for 5 min and then extruding with a 400 nm membrane 20 times. For the confirmation of catalase conjugation on the ONP, catalase was pre-labeled with fluorescein isothiocyanate (FITC) and imaged by using an Olympus FV1200 scanning confocal microscope (Olympus). To confirm the CST functionalized on ILTONP, the ILTONP was observed using a Zeiss LSM 880 II Airyscan FAST confocal microscope.

Evaluating Oxygen Release Profiles of ILTONP.

The oxygen release profiles were detected by employing tris-(bathophenanthroline) ruthenium chloride (GFS chemicals) as an oxygen-sensitive dye and rhodamine B base as a reference dye according to a reported method.^{61,76} Briefly, the dyes were first encapsulated into a polydimethylsiloxane (PDMS) membrane. The membrane was punched, placed into a black 96-well plate, and then balanced in a hypoxic environment (1% O_2) for 24 h. After 200 μL of oxygen-releasing nanoparticles (10 mg/mL in DPBS) was added into each well ($n = 6$), the plate was incubated at 37 °C in a 1% O_2 incubator for 28 days. At each time point, the fluorescence intensities for both tris(bathophenanthroline) ruthenium chloride ($\lambda_{\text{ex/em}} = 470/610$ nm) and rhodamine-B ($\lambda_{\text{ex/em}} = 543/576$ nm) were determined using a SpectraMax iD3 plate reader (Molecular Devices), and the oxygen level was calculated based on the calibration curve.

Particle Size, Morphology, and Stability Analysis.

The size distributions of EXO and ILTEXO were analyzed by nanoparticle tracking analysis (NTA) on a NanoSight NS300 instrument (Malvern Panalytical). The particle size and zeta potential of ONP and ILTONP were determined by dynamic light scattering (DLS) on a Malvern Zetasizer Nano-ZS device. Morphology of the exosomes and oxygen-releasing

nanoparticles was imaged with a JEOL JEM-1400Plus transmission electron microscope (TEM). To evaluate the stability of the ILTEXO and ILTONP, the particles were incubated in a 37 °C simulated body fluid comprised of sodium chloride (8.035 g/L), sodium bicarbonate (0.355 g/L), potassium chloride (0.225 g/L), potassium phosphate dibasic trihydrate (0.231 g/L), magnesium chloride hexahydrate (0.311 g/L), 1 M hydrochloric acid (39 mL/L), calcium chloride (0.292 g/L), sodium sulfate (0.072 g/L), and tris(hydroxymethyl) aminomethane (6.118 g/L). After 28 days, the particle size and morphology were analyzed.

Cell Uptake of ILTEXO and ILTONP.

To evaluate the cellular uptake of ILTEXO and ILTONP, C2C12 cells, HUVECs, and THP-1 derived macrophages were used. C2C12 cells and HUVECs were seeded into collagen-coated 24-well plates at a density of 3×10^4 cells/well. After 24 h, 0.1 mg/mL exosomes or 10 mg/mL oxygen-releasing nanoparticles were added into the wells. To determine uptake by THP-1 derived macrophages, THP-1 cells were cultured in collagen-coated 24-well plates (2×10^5 cells/well) using the culture medium with 100 ng/mL phorbol 12-myristate 13-acetate (PMA).⁷⁷ After 3 days, the medium was removed, and DMEM containing 0.1 mg/mL of exosomes or 10 mg/mL of oxygen-releasing nanoparticles was added ($n = 6$). The plates were then placed in a 1% O₂ incubator. Following 2 h of incubation, the 3 types of cells were stained with Phalloidin-iFluor 488 conjugate (Abcam) and 4',6-diamidino-2-phenylindole (DAPI), respectively. Finally, the stained cells were observed using an Olympus FV1200 scanning confocal microscope (Olympus). Cell uptake ratios were calculated from the percentage of cells with exosomes or oxygen-releasing nanoparticles inside.

Hemocompatibility Assay.

The hemocompatibility of the ILTEXO and ILTONP was evaluated in terms of their thromboresistance.^{33,35} Defibrinated bovine blood (Sigma-Aldrich) was diluted with DPBS in a 1:9 ratio. 0.5 mL of the blood was mixed with 1 mL of DI water, PBS, ILTEXO (0.1 mg/mL), or ILTONP (10 mg/mL). 0.1 M CaCl₂ solution was then added. The samples were incubated at 37 °C for 2 h, followed by centrifugation. The supernatants were dispersed in DI water to release hemoglobin from free red blood cells without being trapped in the blood clots. The absorbance of hemoglobin was detected using a SpectraMax iD3 plate reader (Molecular Devices).

Cell Survival under Hypoxia.

The effect of ILTEXO and ILTONP on the cell survival of C2C12 cells and HUVECs under hypoxia was determined using a Quant-iT PicoGreen dsDNA Assay Kit (Invitrogen).^{78,79} Briefly, C2C12 cells or HUVECs were seeded in 96-well plates at a density of 5×10^2 or 6×10^3 cells/well, respectively. After 24 h of culture under 21% O₂, the medium was replaced with 200 μ L of DMEM containing 0.1 mg/mL of ILTEXO, 10 mg/mL of ILTONP, or both ($n = 6$). The cells were further cultured in a 1% O₂ incubator for 5 days. Then the cells were lysed with papain solution at 60 °C for 24 h. 50 μ L of cell lysis was used for a PicoGreen dsDNA assay and determined on a SpectraMax iD3 plate reader (Molecular Devices) with excitation wavelength and emission wavelength at 480 and 520 nm, respectively.

Cell Migration under Hypoxia.

The effect of ILTEXO and ILTONP on the cell migration of C2C12 cells and HUVECs under hypoxia was evaluated using a scratch assay.^{80,81} C2C12 cells or HUVECs were seeded into a 6-well plate at a density of 3×10^5 cells/well and cultured in the 21% O₂ condition. After the cells formed a confluent monolayer, a straight gap was made by a 200 μ L pipet tip. The cells were then treated with 2 mL of DMEM containing 0.1 mg/mL ILTEXO, 10 mg/mL ILTONP, or both (n = 6). The cells were cultured under 1% O₂ for 24 h. At 0, 12, and 24 h, the scratches were photographed using an EVOS microscope (Olympus), and the images were quantitatively analyzed via ImageJ software. The relative wound area was calculated from the following formula.

$$\begin{aligned} & \text{Relative wound area(\%)} \\ &= \frac{\text{Remained scratch areas at each time point}}{\text{Scratch areas at 0 h}} \times 100 \end{aligned}$$

Endothelial Tube Formation under Hypoxia.

The effect of ILTEXO and ILTONP on the tube formation of HUVECs under hypoxia was investigated using a 2D collagen model.^{82,83} Type I soluble collagen solution (Corning) was diluted with DMEM to a final concentration of 2 mg/mL, followed by adjusting the pH to 7.4 using 1 M NaOH solution. 500 μ L of collagen was added into each well of a 24-well plate. After gelation, HUVECs were seeded onto the collagen gel at a density of 5×10^4 cells/well. The serum-free DMEM containing 0.1 mg/mL ILTEXO, 10 mg/mL ILTONP, or both was added to the wells (n = 6). After incubation under 1% O₂ condition for 24 h, the cells were stained with CellTracker Green CMFDA Dye (Invitrogen) and imaged using an Olympus FV1200 scanning confocal microscope (Olympus). The lumen density was quantified.

Myotube Formation under Hypoxia.

To assess the effect of ILTEXO and ILTONP on myotube formation of C2C12 cells under hypoxia, the cells were seeded into collagen-coated 24-well plates (5×10^4 cells/well) and incubated at 21% O₂. After reaching ~80% confluence, the medium was replaced with DMEM supplemented with 2% horse serum (Gibco). 0.1 mg/mL ILTEXO, 10 mg/mL ILTONP, or both were added into the medium (n = 6). After 5 days of culture, the cells were stained by antimyosin heavy chain antibody (MHC, R&D systems) and DAPI and imaged using an Olympus FV1200 scanning confocal microscope (Olympus). The myotubes with five or more nuclei were quantified.

Western Blotting Analysis.

Protein lysates from C2C12 cells cultured under 1% O₂ with different treatments for 24 h were separated by sodium dodecyl sulfate-polyacrylamide gel electrophoresis (SDS-PAGE) and were subsequently transferred onto Immun-Blot polyvinylidene fluoride (PVDF) membranes (Bio-Rad). The membranes were incubated first with primary antibodies, including p44/42 MAPK (Erk1/2) Rabbit mAb (Cell Signaling Technology, dilution of

1:1000), Phospho-p44/42 MAPK (Erk1/2) Antibody (Cell Signaling Technology, dilution of 1:1000), Akt (pan) (C67E7) Rabbit mAb (Cell Signaling Technology, dilution of 1:1000), Phospho-Akt Antibody (Cell Signaling Technology, dilution of 1:1000), or GAPDH (14C10) Rabbit mAb (Cell Signaling Technology, dilution of 1:1000), and then appropriate HRP-conjugated secondary antibodies. The immunoblots were imaged by using a ChemiDoc XRS+ Gel Imaging System (Bio-Rad).

Critical Limb Ischemia Model in Diabetic Mice.

All animal experiments were carried out in conformance with the Guide for the Care and Use of Laboratory Animals of the National Institutes of Health and approved by the Institutional Animal Care and Use Committee of Washington University in St. Louis. Critical limb ischemia surgery was performed on female db/db mice aged 8–10 weeks (Jackson Laboratory). Under anesthesia with 2% isoflurane, one hindlimb of each mouse was ligated with a 6.0 silk thread at both the proximal and distal portions of the left femoral artery and vein, and the vessels were completely severed between the two sutures.^{73–75} The contralateral hindlimb served as a control. 4 h after the surgery, the mice were randomly divided into five groups ($n = 6$ for each group), each of which was intravenously injected with 200 μL of PBS (PBS group), 10 mg/mL of empty nanoparticles in PBS (NP group), 0.3 mg/mL of ILTEXO in PBS (ILTEXO group), 10 mg/mL of ILTONP in PBS (ILTONP group), or ILTEXO and ILTONP (ILTEXO/ILTONP group).

Biodistribution of ILTEXO and ILTONP.

4 h after the surgery, the mice were intravenously injected with 200 μL of PBS, 0.3 mg/mL of ILTEXO, or 10 mg/mL of ILTONP. After 2 days, the mice were euthanized, and both hindlimbs together with major organs (heart, lung, liver, spleen, and kidney) were harvested for ex vivo imaging with an IVIS 50 *In Vivo* Bioluminescence Imaging System (PerkinElmer) with dsRed emission filter. The acquired images were analyzed by using Living Image 4.4 software.

Blood Perfusion Measurement.

The blood perfusion of the hindlimbs with and without surgery was monitored using a laser Doppler imager (Perimed) on days 0, 1, 7, 14, 21, and 28. The resulting images were analyzed to quantify the blood perfusion. The ratio of blood perfusion between the surgery hindlimb and the contralateral hindlimb was calculated.^{84,85}

Histology and Immunohistochemistry Analysis.

On day 28 after surgery, the mice were sacrificed, and the ischemic hindlimbs were collected. For histology and immunohistochemistry analysis, the harvested hindlimbs were fixed with 4% paraformaldehyde solution (PFA, Thermo scientific), embedded in paraffin, and sectioned into 5 μm slices. To evaluate the microanatomy of skeletal muscles, the tissue sections were stained with hematoxylin and eosin (H&E) and imaged using a Zeiss LSM 880 Confocal Microscope under bright field illumination. To determine collagen distribution, PicroSirius Red staining was performed, and the images were taken using a Zeiss Axio Imager 2 with polarized light illumination.

For immunohistochemistry staining, the paraffin sections were deparaffinized and underwent heat-induced epitope retrieval in Trisethylenediaminetetraacetic acid (EDTA) buffer (pH = 8), blocked with 10% goat serum and 0.3% Triton X-100 in 1X DPBS, and then incubated with primary antibodies at 4 °C overnight. The antibodies included anti-Ki67 antibody (Abcam, dilution of 1:200), anti-PGC1- α antibody (Abcam, dilution of 1:200), biotin-XX isolectin GS-IB4 conjugate (Invitrogen, dilution of 1:100), anti- α -SMA antibody (dilution of 1:100, ab5694, Abcam), myosin heavy chain (MHC) antibody (R&D systems, dilution of 1:50), anti-MyoD1 antibody (Abcam, dilution of 1:100), anti-Pax-7 antibody (Santa Cruz Biotechnology, dilution of 1:50), anti-CD68 antibody (Abcam, dilution of 1:500), and antimannose receptor antibody (CD206, Abcam, dilution of 1:9000), respectively. After being stained with the corresponding Alexa Fluor 488- or 647-conjugated secondary antibodies (Invitrogen) and Hoechst 33342, the tissue sections were imaged with a Zeiss LSM 880 confocal microscope.

Cell apoptosis in ischemic areas was assessed by using a Click-iT Plus TUNEL Assay for In Situ Apoptosis Detection Kit (Invitrogen) following the manufacturer's instructions. ROS levels in the tissues were detected with a CM-H2DCFDA (General Oxidative Stress Indicator, Invitrogen).^{35,86} The stained tissues were visualized with a Zeiss LSM 880 Confocal Microscope.

mRNA Expression Analysis.

To determine the mRNA expression in ischemic muscles, 4 weeks after treatments, ischemic hindlimbs were harvested, and total RNA was extracted from homogenized muscle samples using Trizol (Invitrogen) and then converted to cDNA using a High Capacity cDNA Reverse Transcription Kit (Applied Biosystems). Gene expressions of Vegfa and Fgf2 were determined using a Maxima SYBR Green/ROX qPCR Master Mix (Thermo Scientific) on a QuantStudio 5 Real-Time PCR Detection System (Applied Biosystems). The primers for Actb, Vegfa, and Fgf2 were shown in Table S1. The real-time qPCR conditions were as follows: 50 °C for 2 min, 95 °C for 10 min, followed by 40 cycles of 95 °C for 15 s and 60 °C for 1 min. β -Actin served as the housekeeping gene, and the relative mRNA expression was calculated according to a standard Ct method.

Statistical Analysis.

The data are displayed as mean \pm standard deviation. Statistical significance was calculated by one-way ANOVA. Significance was defined as $p < 0.05$.

Supplementary Material

Refer to Web version on PubMed Central for supplementary material.

ACKNOWLEDGMENTS

We thank Dr. Xiaolei Nie for performing partial animal surgeries and laser Doppler imaging. Confocal imaging was conducted in the Washington University Center for Cellular Imaging (WUCCI), which is supported by Washington University School of Medicine, The Children's Discovery Institute of Washington University and St. Louis Children's Hospital (CDI-CORE-2015-505 and CDI-CORE-2019-813), and the Foundation for Barnes-Jewish Hospital (3770 and 4642). Histological sectioning was performed in the Musculoskeletal Research Center in Washington University School of Medicine. IVIS characterization was conducted by the Molecular Imaging Center

in Washington University School of Medicine. We thank J. Ballard from the Engineering Communication Center in Washington University for editing the manuscript.

Funding

This work was supported by US National Institutes of Health (R01HL138175, R01HL138353, R01EB022018, R01AG056919, R01HL164062, and R01DK133949).

REFERENCES

- (1). Golledge J Update on the Pathophysiology and Medical Treatment of Peripheral Artery Disease. *Nat. Rev. Cardiol* 2022, 19, 456–474. [PubMed: 34997200]
- (2). Aday AW; Matsushita K Epidemiology of Peripheral Artery Disease and Polyvascular Disease. *Circ. Res* 2021, 128, 1818–1832. [PubMed: 34110907]
- (3). Takahara M Diabetes Mellitus and Lower Extremity Peripheral Artery Disease. *JMA J* 2021, 4, 225–231. [PubMed: 34414316]
- (4). Soyoye DO; Abiodun OO; Ikem RT; Kolawole BA; Akintomide AO Diabetes and Peripheral Artery Disease: A Review. *World J. Diabetes* 2021, 12, 827–838. [PubMed: 34168731]
- (5). Ruetenapf G; Morbach S; Sigl M. J. J. o. C. M. Therapeutic Alternatives in Diabetic Foot Patients without an Option for Revascularization: A Narrative Review. *J. Clin. Med* 2022, 11, 2155. [PubMed: 35456247]
- (6). Benedetto F; Spinelli D; Pipito N; Barilla D; Stilo F; De Caridi G; Barilla C; Spinelli F Inframalleolar Bypass for Chronic Limb-Threatening Ischemia. *Vasc. Med* 2021, 26, 187–194. [PubMed: 33407009]
- (7). Steiner S; Schmidt A Endovascular Interventions for Peripheral Arterial Disease. *Inn Med. (Heidelb)* 2022, 63, 584–590. [PubMed: 35532802]
- (8). Beckman JA; Schneider PA; Conte MS Advances in Revascularization for Peripheral Artery Disease: Revascularization in Pad. *Circ. Res* 2021, 128, 1885–1912. [PubMed: 34110904]
- (9). Magenta A; Florio MC; Ruggeri M; Furgiuele S Autologous Cell Therapy in Diabetes-Associated Critical Limb Ischemia: From Basic Studies to Clinical Outcomes. *Int. J. Mol. Med* 2021, 48, 1–18.
- (10). Ohtake T; Mochida Y; Ishioka K; Oka M; Maesato K; Moriya H; Hidaka S; Higashide S; Ioji T; Fujita Y; Kawamoto A; Fukushima M; Kobayashi S Autologous Granulocyte Colony-Stimulating Factor-Mobilized Peripheral Blood Cd34 Positive Cell Transplantation for Hemodialysis Patients with Critical Limb Ischemia: A Prospective Phase Ii Clinical Trial. *Stem Cells Transl. Med* 2018, 7, 774–782. [PubMed: 30059194]
- (11). Lu D; Jiang Y; Deng W; Zhang Y; Liang Z; Wu Q; Jiang X; Zhang L; Gao F; Cao Y; Chen B; Xue Y Long-Term Outcomes of Bmmsc Compared with Bmmnc for Treatment of Critical Limb Ischemia and Foot Ulcer in Patients with Diabetes. *Cell Transplant* 2019, 28, 645–652. [PubMed: 30917698]
- (12). Sharma S; Pandey NN; Sinha M; Kumar S; Jagia P; Gulati GS; Gond K; Mohanty S; Bhargava B Randomized, Double-Blind, Placebo-Controlled Trial to Evaluate Safety and Therapeutic Efficacy of Angiogenesis Induced by Intraarterial Autologous Bone Marrow-Derived Stem Cells in Patients with Severe Peripheral Arterial Disease. *J. Vasc. Interv. Radiol* 2021, 32, 157–163. [PubMed: 33248918]
- (13). Yong KW; Choi JR; Mohammadi M; Mitha AP; Sanati-Nezhad A; Sen A Mesenchymal Stem Cell Therapy for Ischemic Tissues. *Stem Cells Int* 2018, 2018, 8179075. [PubMed: 30402112]
- (14). Liotta F; Annunziato F; Castellani S; Boddi M; Alterini B; Castellini G; Mazzanti B; Cosmi L; Acquafresca M; Bartalesi FJ; et al. Therapeutic Efficacy of Autologous Non-Mobilized Enriched Circulating Endothelial Progenitors in Patients with Critical Limb Ischemia—the Scelta Trial—. *Circulation J* 2018, 82, 1688–1698.
- (15). Lebedev SV; Karasev AV; Kungurtsev VV; Lokhonina AV; Kleimenova EB Cell Therapy of Critical Lower Limb Ischemia (Problems and Prospects). *Vestn. Ross. Akad. Med. Nauk* 2013, 68, 33–44.

- (16). Kang WC; Oh PC; Lee K; Ahn T; Byun K Increasing Injection Frequency Enhances the Survival of Injected Bone Marrow Derived Mesenchymal Stem Cells in a Critical Limb Ischemia Animal Model. *Korean J. Physiol. Pharmacol.* 2016, 20, 657–667.
- (17). Du W; Zhang K; Zhang S; Wang R; Nie Y; Tao H; Han Z; Liang L; Wang D; Liu J; Liu N; Han Z; Kong D; Zhao Q; Li Z Enhanced Proangiogenic Potential of Mesenchymal Stem Cell-Derived Exosomes Stimulated by a Nitric Oxide Releasing Polymer. *Biomaterials* 2017, 133, 70–81. [PubMed: 28433939]
- (18). Hu GW; Li Q; Niu X; Hu B; Liu J; Zhou SM; Guo SC; Lang HL; Zhang CQ; Wang Y; Deng ZF Exosomes Secreted by Human-Induced Pluripotent Stem Cell-Derived Mesenchymal Stem Cells Attenuate Limb Ischemia by Promoting Angiogenesis in Mice. *Stem Cell Res. Ther* 2015, 6, 10. [PubMed: 26268554]
- (19). Ju C; Li Y; Shen Y; Liu Y; Cai J; Liu N; Ma G; Tang Y Transplantation of Cardiac Mesenchymal Stem Cell-Derived Exosomes for Angiogenesis. *J. Cardiovasc. Transl. Res* 2018, 11, 429–437. [PubMed: 30276617]
- (20). Mathiyalagan P; Liang Y; Kim D; Misener S; Thorne T; Kamide CE; Klyachko E; Losordo DW; Hajjar RJ; Sahoo S Angiogenic Mechanisms of Human Cd34(+) Stem Cell Exosomes in the Repair of Ischemic Hindlimb. *Circ. Res* 2017, 120, 1466–1476. [PubMed: 28298297]
- (21). Ye M; Ni Q; Qi H; Qian X; Chen J; Guo X; Li M; Zhao Y; Xue G; Deng H; Zhang L Exosomes Derived from Human Induced Pluripotent Stem Cells-Endothelial Cells Promotes Postnatal Angiogenesis in Mice Bearing Ischemic Limbs. *Int. J. Biol. Sci* 2019, 15, 158–168. [PubMed: 30662356]
- (22). Zhu Q; Li Q; Niu X; Zhang G; Ling X; Zhang J; Wang Y; Deng Z Extracellular Vesicles Secreted by Human Urine-Derived Stem Cells Promote Ischemia Repair in a Mouse Model of Hind-Limb Ischemia. *Cell Physiol. Biochem* 2018, 47, 1181–1192. [PubMed: 30041250]
- (23). Anderson JD; Johansson HJ; Graham CS; Vesterlund M; Pham MT; Bramlett CS; Montgomery EN; Mellema MS; Bardini RL; Contreras Z; Hoon M; Bauer G; Fink KD; Fury B; Hendrix KJ; Chedin F; El-Andaloussi S; Hwang B; Mulligan MS; Lehtiö J; et al. Comprehensive Proteomic Analysis of Mesenchymal Stem Cell Exosomes Reveals Modulation of Angiogenesis Via Nuclear Factor- κ B Signaling. *Stem Cells* 2016, 34, 601–613. [PubMed: 26782178]
- (24). Gu Y; Rampin A; Alvino VV; Spinetti G; Madeddu P Cell Therapy for Critical Limb Ischemia: Advantages, Limitations, and New Perspectives for Treatment of Patients with Critical Diabetic Vasculopathy. *Current diabetes reports* 2021, 21, 11. [PubMed: 33651185]
- (25). Yan B; Zhang Y; Liang C; Liu B; Ding F; Wang Y; Zhu B; Zhao R; Yu XY; Li Y Stem Cell-Derived Exosomes Prevent Pyroptosis and Repair Ischemic Muscle Injury through a Novel Exosome/Circhipk3/Foxo3a Pathway. *Theranostics* 2020, 10, 6728–6742. [PubMed: 32550900]
- (26). Johnson TK; Zhao L; Zhu D; Wang Y; Xiao Y; Oguljahan B; Zhao X; Kirlin WG; Yin L; Chilian WM; Liu D Exosomes Derived from Induced Vascular Progenitor Cells Promote Angiogenesis in Vitro and in an in Vivo Rat Hindlimb Ischemia Model. *Am. J. Physiol. Heart Circ. Physiol* 2019, 317, H765–h776. [PubMed: 31418583]
- (27). Zhu D; Johnson TK; Wang Y; Thomas M; Huynh K; Yang Q; Bond VC; Chen YE; Liu D Macrophage M2 Polarization Induced by Exosomes from Adipose-Derived Stem Cells Contributes to the Exosomal Proangiogenic Effect on Mouse Ischemic Hindlimb. *Stem Cell Res. Ther* 2020, 11, 162. [PubMed: 32321589]
- (28). Liang Y; Duan L; Lu J; Xia J Engineering Exosomes for Targeted Drug Delivery. *Theranostics* 2021, 11, 3183–3195. [PubMed: 33537081]
- (29). Elsharkasy OM; Nordin JZ; Hagey DW; de Jong OG; Schiffelers RM; Andaloussi SE; Vader P Extracellular Vesicles as Drug Delivery Systems: Why and How? *Adv. Drug Delivery Rev* 2020, 159, 332–343.
- (30). Wu P; Zhang B; Ocansey DKW; Xu W; Qian H Extracellular Vesicles: A Bright Star of Nanomedicine. *Biomaterials* 2021, 269, 120467. [PubMed: 33189359]
- (31). An T; Chen Y; Tu Y; Lin P Mesenchymal Stromal Cell-Derived Extracellular Vesicles in the Treatment of Diabetic Foot Ulcers: Application and Challenges. *Stem Cell Rev. Rep* 2021, 17, 369–378. [PubMed: 32772239]

- (32). Li X; Xie X; Lian W; Shi R; Han S; Zhang H; Lu L; Li M Exosomes from Adipose-Derived Stem Cells Overexpressing Nrf2 Accelerate Cutaneous Wound Healing by Promoting Vascularization in a Diabetic Foot Ulcer Rat Model. *Exp. Mol. Med* 2018, 50, 1–14.
- (33). Dang Y; Gao N; Niu H; Guan Y; Fan Z; Guan J Targeted Delivery of a Matrix Metalloproteinases-2 Specific Inhibitor Using Multifunctional Nanogels to Attenuate Ischemic Skeletal Muscle Degeneration and Promote Revascularization. *ACS Appl. Mater. Interfaces* 2021, 13, 5907–5918. [PubMed: 33506676]
- (34). Kanki S; Jaalouk DE; Lee S; Yu AYC; Gannon J; Lee RT Identification of Targeting Peptides for Ischemic Myocardium by in Vivo Phage Display. *J. Mol. Cell. Cardiol* 2011, 50, 841–848. [PubMed: 21316369]
- (35). Guan Y; Niu H; Wen J; Dang Y; Zayed M; Guan J Rescuing Cardiac Cells and Improving Cardiac Function by Targeted Delivery of Oxygen-Releasing Nanoparticles after or Even before Acute Myocardial Infarction. *ACS Nano* 2022, 16, 19551–19566. [PubMed: 36367231]
- (36). Hu S; Wang X; Li Z; Zhu D; Cores J; Wang Z; Li J; Mei X; Cheng X; Su T; Cheng K Platelet Membrane and Stem Cell Exosome Hybrids Enhance Cellular Uptake and Targeting to Heart Injury. *Nano Today* 2021, 39, 101210. [PubMed: 34306170]
- (37). Wang X; Chen Y; Zhao Z; Meng Q; Yu Y; Sun J; Yang Z; Chen Y; Li J; Ma T; Liu H; Li Z; Yang J; Shen Z Engineered Exosomes with Ischemic Myocardium-Targeting Peptide for Targeted Therapy in Myocardial Infarction. *J. Am. Heart Assoc* 2018, 7, No. e008737. [PubMed: 30371236]
- (38). Mouw JK; Ou G; Weaver VM Extracellular Matrix Assembly: A Multiscale Deconstruction. *Nat. Rev. Mol. Cell Biol* 2014, 15, 771–785. [PubMed: 25370693]
- (39). Lippi G; Franchini M; Targher G Arterial Thrombus Formation in Cardiovascular Disease. *Nat. Rev. Cardiol* 2011, 8, 502–512. [PubMed: 21727917]
- (40). Tang J; Su T; Huang K; Dinh P-U; Wang Z; Vandergriff A; Hensley MT; Cores J; Allen T; Li T; et al. Targeted Repair of Heart Injury by Stem Cells Fused with Platelet Nanovesicles. *Nat. Biomed. Eng* 2018, 2, 17–26. [PubMed: 29862136]
- (41). Hu C-MJ; Fang RH; Wang K-C; Luk BT; Thamphiwatana S; Dehaini D; Nguyen P; Angsantikul P; Wen CH; Kroll AV; et al. Nanoparticle Biointerfacing by Platelet Membrane Cloaking. *Nature* 2015, 526, 118–121. [PubMed: 26374997]
- (42). Manning BD; Toker A Akt/Pkb Signaling: Navigating the Network. *Cell* 2017, 169, 381–405. [PubMed: 28431241]
- (43). Gangadaran P; Rajendran RL; Lee HW; Kalimuthu S; Hong CM; Jeong SY; Lee S-W; Lee J; Ahn B-C Extracellular Vesicles from Mesenchymal Stem Cells Activates Vegf Receptors and Accelerates Recovery of Hindlimb Ischemia. *J. Controlled Release* 2017, 264, 112–126.
- (44). Wen X; Jiao L; Tan H Mapk/Erk Pathway as a Central Regulator in Vertebrate Organ Regeneration. *Int. J. Mol. Sci* 2022, 23, 1464. [PubMed: 35163418]
- (45). Beckman JA; Paneni F; Cosentino F; Creager MA Diabetes and Vascular Disease: Pathophysiology, Clinical Consequences, and Medical Therapy: Part II. *Eur. Heart J* 2013, 34, 2444–2452. [PubMed: 23625211]
- (46). Spreen MI; Gremmels H; Teraa M; Sprengers RW; Verhaar MC; Stadius van Eps RG; de Vries JP; Mali WP; van Overhagen H Diabetes Is Associated with Decreased Limb Survival in Patients with Critical Limb Ischemia: Pooled Data from Two Randomized Controlled Trials. *Diabetes care* 2016, 39, 2058–2064. [PubMed: 27612499]
- (47). Li JY; Yang XY; Wang XF; Jia X; Wang ZJ; Deng AP; Bai XL; Zhu L; Li BH; Feng ZB; Li Y; Wang L; Jin S Siglec-5 Is a Novel Marker of Critical Limb Ischemia in Patients with Diabetes. *Sci. Rep* 2017, 7, 11272. [PubMed: 28900239]
- (48). Brownlee M The Pathobiology of Diabetic Complications: A Unifying Mechanism. *Diabetes* 2005, 54, 1615–1625. [PubMed: 15919781]
- (49). Edsfeldt A; Gonçalves I; Grufman H; Nitulescu M; Dunér P; Bengtsson E; Mollet IG; Persson A; Nilsson M; Orho-Melander M; Melander O; Björkbacka H; Nilsson J Impaired Fibrous Repair: A Possible Contributor to Atherosclerotic Plaque Vulnerability in Patients with Type II Diabetes. *Arterioscler., Thromb., Vasc. Biol* 2014, 34, 2143–2150. [PubMed: 25035341]

- (50). Hirata Y; Nomura K; Senga Y; Okada Y; Kobayashi K; Okamoto S; Minokoshi Y; Imamura M; Takeda S; Hosooka T; Ogawa W Hyperglycemia Induces Skeletal Muscle Atrophy Via a Wwp1/Klf15 Axis. *JCI insight* 2019, 4, No. e124952. [PubMed: 30830866]
- (51). Alev C; Ii M; Asahara T Endothelial Progenitor Cells: A Novel Tool for the Therapy of Ischemic Diseases. *Antioxid. Redox Signaling* 2011, 15, 949–965.
- (52). Benoit E; O'Donnell TF; Patel AN Safety and Efficacy of Autologous Cell Therapy in Critical Limb Ischemia: A Systematic Review. *Cell Transplant* 2013, 22, 545–562. [PubMed: 22490340]
- (53). Gupta NK; Armstrong EJ; Parikh SA The Current State of Stem Cell Therapy for Peripheral Artery Disease. *Curr. Cardiol. Rep* 2014, 16, 447. [PubMed: 24414120]
- (54). Hart CA; Tsui J; Khanna A; Abraham DJ; Baker DM Stem Cells of the Lower Limb: Their Role and Potential in Management of Critical Limb Ischemia. *Exp. Biol. Med. (Maywood)* 2013, 238, 1118–1126. [PubMed: 23996960]
- (55). Jadowiec C; Brenes RA; Li X; Lv W; Protack CD; Collins MJ; Dardik A Stem Cell Therapy for Critical Limb Ischemia: What Can We Learn from Cell Therapy for Chronic Wounds? *Vascular* 2012, 20, 284–289. [PubMed: 23086986]
- (56). Liew A; O'Brien T Therapeutic Potential for Mesenchymal Stem Cell Transplantation in Critical Limb Ischemia. *Stem Cell Res. Ther* 2012, 3, 28. [PubMed: 22846185]
- (57). Raval Z; Losordo DW Cell Therapy of Peripheral Arterial Disease: From Experimental Findings to Clinical Trials. *Circ. Res* 2013, 112, 1288–1302. [PubMed: 23620237]
- (58). Huang C; Luo W; Wang Q; Ye Y; Fan J; Lin L; Shi C; Wei W; Chen H; Wu Y; Tang Y Human Mesenchymal Stem Cells Promote Ischemic Repairment and Angiogenesis of Diabetic Foot through Exosome Mirna-21–5p. *Stem Cell Res* 2021, 52, 102235. [PubMed: 33601096]
- (59). Zhang K; Li Z Molecular Imaging of Therapeutic Effect of Mesenchymal Stem Cell-Derived Exosomes for Hindlimb Ischemia Treatment. *Methods Mol. Biol* 2019, 2150, 213–225.
- (60). Zhang X; Jiang Y; Huang Q; Wu Z; Pu H; Xu Z; Li B; Lu X; Yang X; Qin J; Peng Z Exosomes Derived from Adipose-Derived Stem Cells Overexpressing Glyoxalase-1 Protect Endothelial Cells and Enhance Angiogenesis in Type 2 Diabetic Mice with Limb Ischemia. *Stem Cell Res. Ther* 2021, 12, 403. [PubMed: 34266474]
- (61). Guan Y; Gao N; Niu H; Dang Y; Guan J Oxygen-Release Microspheres Capable of Releasing Oxygen in Response to Environmental Oxygen Level to Improve Stem Cell Survival and Tissue Regeneration in Ischemic Hindlimbs. *J. Controlled Release* 2021, 331, 376–389.
- (62). Bloor AJC; Patel A; Griffin JE; Gilleece MH; Radia R; Yeung DT; Drier D; Larson LS; Uenishi GI; Hei D; Kelly K; Slukvin I; Rasko JEJ Production, Safety and Efficacy of Ipsc-Derived Mesenchymal Stromal Cells in Acute Steroid-Resistant Graft Versus Host Disease: A Phase I, Multicenter, Open-Label, Dose-Escalation Study. *Nat. Med* 2020, 26, 1720–1725. [PubMed: 32929265]
- (63). Gao W; He R; Ren J; Zhang W; Wang K; Zhu L; Liang T Exosomal Hmgbl Derived from Hypoxia-Conditioned Bone Marrow Mesenchymal Stem Cells Increases Angiogenesis Via the Jnk/Hif-1 α Pathway. *FEBS open bio* 2021, 11, 1364–1373.
- (64). Sun L; Zhu W; Zhao P; Wang Q; Fan B; Zhu Y; Lu Y; Chen Q; Zhang J; Zhang F Long Noncoding Rna Uca1 from Hypoxia-Conditioned Hmsc-Derived Exosomes: A Novel Molecular Target for Cardioprotection through Mir-873–5p/Xiap Axis. *Cell Death Dis* 2020, 11, 696. [PubMed: 32826854]
- (65). Almeria C; Weiss R; Roy M; Tripisciano C; Kasper C; Weber V; Egger D Hypoxia Conditioned Mesenchymal Stem Cell-Derived Extracellular Vesicles Induce Increased Vascular Tube Formation in Vitro. *Front. Bioeng. Biotechnol* 2019, 7, 292. [PubMed: 31709251]
- (66). Zhu L-P; Tian T; Wang J-Y; He J-N; Chen T; Pan M; Xu L; Zhang H.-x.; Qiu X-T; Li C-C; et al. Hypoxia-Elicited Mesenchymal Stem Cell-Derived Exosomes Facilitates Cardiac Repair through Mir-125b-Mediated Prevention of Cell Death in Myocardial Infarction. *Theranostics* 2018, 8, 6163. [PubMed: 30613290]
- (67). Zamocky M; Furtmüller PG; Obinger C Evolution of Catalases from Bacteria to Humans. *Antioxid. Redox Signaling* 2008, 10, 1527–1548.
- (68). Chelikani P; Fita I; Loewen PC Diversity of Structures and Properties among Catalases. *Cell. Mol. Life Sci* 2004, 61, 192–208. [PubMed: 14745498]

- (69). Harrison BS; Eberli D; Lee SJ; Atala A; Yoo JJ Oxygen Producing Biomaterials for Tissue Regeneration. *Biomaterials* 2007, 28, 4628–4634. [PubMed: 17681597]
- (70). Pedraza E; Coronel MM; Fraker CA; Ricordi C; Stabler CL Preventing Hypoxia-Induced Cell Death in Beta Cells and Islets Via Hydrolytically Activated, Oxygen-Generating Biomaterials. *Proc. Natl. Acad. Sci. U.S.A* 2012, 109, 4245–4250. [PubMed: 22371586]
- (71). Oh SH; Ward CL; Atala A; Yoo JJ; Harrison BS Oxygen Generating Scaffolds for Enhancing Engineered Tissue Survival. *Biomaterials* 2009, 30, 757–762. [PubMed: 19019425]
- (72). Zhang X; Zhang Y; Zhang R; Jiang X; Midgley AC; Liu Q; Kang H; Wu J; Khalique A; Qian M; et al. Biomimetic Design of Artificial Hybrid Nanocells for Boosted Vascular Regeneration in Ischemic Tissues. *Adv. Mater* 2022, 34, 2110352.
- (73). Matsakas A; Yadav V; Lorca S; Evans RM; Narkar VA Revascularization of Ischemic Skeletal Muscle by Estrogen-Related Receptor- Γ . *Circ. Res* 2012, 110, 1087–1096. [PubMed: 22415017]
- (74). Zhu Q; Liu X; Zhu Q; Liu Z; Yang C; Wu H; Zhang L; Xia X; Wang M; Hao H; Cui Y; Zhang G; Hill MA; Flaker GC; Zhou S; Liu Z N-Acetylcysteine Enhances the Recovery of Ischemic Limb in Type-2 Diabetic Mice. *Antioxidants (Basel)* 2022, 11, 1097. [PubMed: 35739993]
- (75). Xu Y; Fu M; Li Z; Fan Z; Li X; Liu Y; Anderson PM; Xie X; Liu Z; Guan J A Prosurvival and Proangiogenic Stem Cell Delivery System to Promote Ischemic Limb Regeneration. *Acta Biomater* 2016, 31, 99–113. [PubMed: 26689466]
- (76). Guan Y; Niu H; Wen J; Dang Y; Zayed M; Guan J Rescuing Cardiac Cells and Improving Cardiac Function by Targeted Delivery of Oxygen-Releasing Nanoparticles after or Even before Acute Myocardial Infarction. *ACS Nano* 2022, 16, 19551–19556. [PubMed: 36367231]
- (77). Lunov O; Syrovets T; Loos C; Beil J; Delacher M; Tron K; Nienhaus GU; Musyanovych A; Mailander V; Landfester K; Simmet T Differential Uptake of Functionalized Polystyrene Nanoparticles by Human Macrophages and a Monocytic Cell Line. *ACS Nano* 2011, 5, 1657–1669. [PubMed: 21344890]
- (78). Yang Y; Zhu Z; Gao R; Yuan J; Zhang J; Li H; Xie Z; Wang Y Controlled Release of Msc-Derived Small Extracellular Vesicles by an Injectable Diels-Alder Crosslinked Hyaluronic Acid/Peg Hydrogel for Osteoarthritis Improvement. *Acta Biomater* 2021, 128, 163–174. [PubMed: 33862283]
- (79). Lee J; Lee S; Ahmad T; Madhurakkat Perikamana SK; Lee J; Kim EM; Shin H Human Adipose-Derived Stem Cell Spheroids Incorporating Platelet-Derived Growth Factor (PDGF) and Bio-Minerals for Vascularized Bone Tissue Engineering. *Biomaterials* 2020, 255, 120192. [PubMed: 32559565]
- (80). Chen Z; Duan J; Diao Y; Chen Y; Liang X; Li H; Miao Y; Gao Q; Gui L; Wang X; et al. ROS-Responsive Capsules Engineered from Egcg-Zinc Networks Improve Therapeutic Angiogenesis in Mouse Limb Ischemia. *Bioact. Mater* 2021, 6, 1–11. [PubMed: 32817909]
- (81). Zou Y; Li L; Li Y; Chen S; Xie X; Jin X; Wang X; Ma C; Fan G; Wang W Restoring Cardiac Functions after Myocardial Infarction-Ischemia/Reperfusion Via an Exosome Anchoring Conductive Hydrogel. *ACS Appl. Mater. Interfaces* 2021, 13, 56892–56908. [PubMed: 34823355]
- (82). Ahn M-R; Kunimasa K; Ohta T; Kumazawa S; Kamihira M; Kaji K; Uto Y; Hori H; Nagasawa H; Nakayama T Suppression of Tumor-Induced Angiogenesis by Brazilian Propolis: Major Component Artepillin C Inhibits *In Vitro* Tube Formation and Endothelial Cell Proliferation. *Cancer Lett* 2007, 252, 235–243. [PubMed: 17343983]
- (83). Cooley LS; Handsley MM; Zhou Z; Lafleur MA; Pennington CJ; Thompson EW; Pöschl E; Edwards DR Reversible Transdifferentiation of Blood Vascular Endothelial Cells to a Lymphatic-Like Phenotype *In Vitro*. *J. Cell Sci* 2010, 123, 3808–3816. [PubMed: 20940254]
- (84). Guan Y; Gao N; Niu H; Dang Y; Guan J Oxygen-Release Microspheres Capable of Releasing Oxygen in Response to Environmental Oxygen Level to Improve Stem Cell Survival and Tissue Regeneration in Ischemic Hindlimbs. *J. Controlled Release* 2021, 331, 376–389.
- (85). Park I-S; Mahapatra C; Park JS; Dashnyam K; Kim J-W; Ahn JC; Chung P-S; Yoon DS; Mandakhbayar N; Singh RK; et al. Revascularization and Limb Salvage Following Critical Limb Ischemia by Nanoceria-Induced Ref-1/Ape1-Dependent Angiogenesis. *Biomaterials* 2020, 242, 119919. [PubMed: 32146371]

- (86). Fan Z; Xu Z; Niu H; Gao N; Guan Y; Li C; Dang Y; Cui X; Liu XL; Duan Y; et al. An Injectable Oxygen Release System to Augment Cell Survival and Promote Cardiac Repair Following Myocardial Infarction. *Sci. Rep* 2018, 8, 1371. [PubMed: 29358595]

Author Manuscript

Author Manuscript

Author Manuscript

Author Manuscript

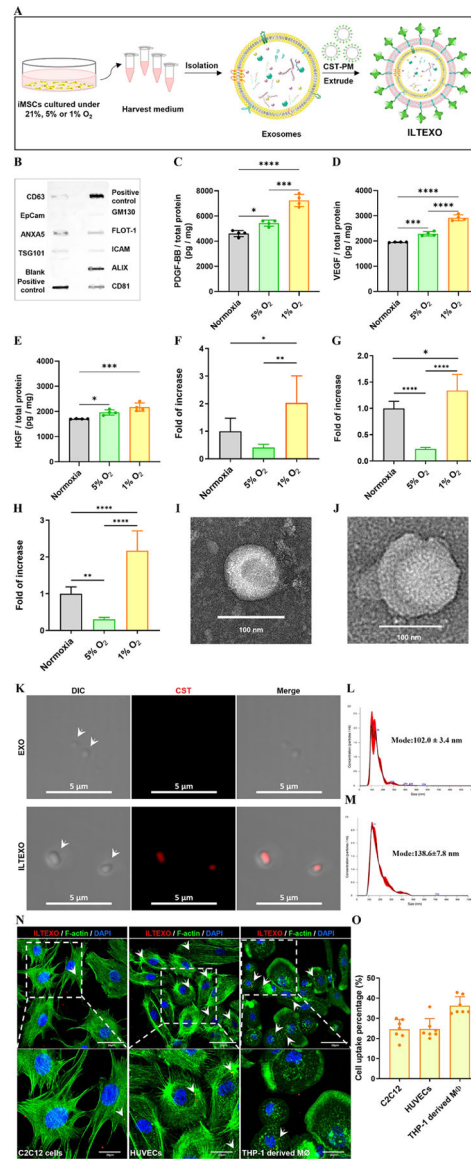


Figure 1. Characterization of iMSC-derived exosomes without modification (EXO) and modified with ischemic-limb-targeting capability (ILTEXO). (A) Schematic illustration of EXO isolation and ILTEXO preparation. (B) Biomarkers on EXO analyzed by using an Exo-Check Exosome Antibody Array. (C–E) Quantitative analysis of angiogenesis-related growth factors, including PDGF-BB (C), VEGF (D), and HGF (E), in exosomes isolated from iMSCs cultured in different oxygen environments ($n = 4$). (F–H) Comparison of miRNA contents, including miR126-3p (F), miR21-5p (G), and miR182-5p (H), in exosomes isolated from iMSCs cultured under hypoxia and normoxia ($n = 6$). (I, J) TEM images of EXO (I) and ILTEXO (J). Scale bar = 100 nm. (K) Fluorescent images (middle) corresponding to differential interference contrast (DIC) images (left) and merged images (right) for both EXO (upper) and ILTEXO (lower); scale bar = 5 μm . The images were taken for aggregated exosomes since confocal microscopes have limited resolution for clearly

imaging a single exosome. (L, M) Size distribution of EXO (L) and ILTEXO (M) using nanoparticle tracking analysis (NTA). (N) Cellular internalization of ILTEXO by C2C12 cells (left), HUVECs (center), and THP-1 derived macrophages (right) after incubation for 2 h under hypoxia (1% O₂). Co-localization of ILTEXO within the cells is denoted in yellow and emphasized by white arrows. Included are scale bars 50 μm for the upper images and 20 μm for the enlarged lower field of views. (O) Quantification of cell uptake efficiency of ILTEXO by three types of cells ($n = 7$). * $p < 0.05$, ** $p < 0.01$, *** $p < 0.001$, **** $p < 0.0001$.

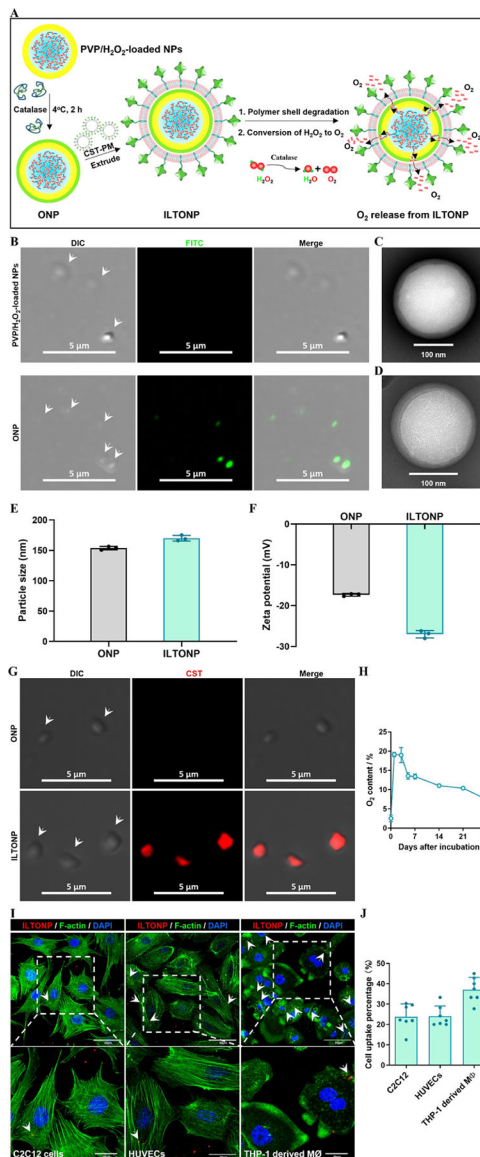


Figure 2. Fabrication and characterizations of ischemic-limb-targeting oxygen-releasing nanoparticles (ILTNP). (A) Schematic representations of ITLONP fabrication and release of O₂ from ILTNP. (B) Fluorescent images (middle) correspond with DIC images (left) and merged images (right) for both PVP/H₂O₂-loaded NPs (top) and ONP (lower). Scale bar = 5 μ m. The images were taken for aggregated nanoparticles since confocal microscopes have limited resolution for clearly imaging a single nanoparticle. (C, D) TEM images of ONP (C) and ILTNP (D); scale bar = 100 nm. Particle size (E) and zeta potential (F) of ONP and ILTNP, measured by dynamic light scattering (DLS), $n = 3$. (G) Fluorescent images (middle), paired with DIC images (left) and their corresponding merged images (right) for both ONP (upper) and ILTNP (lower); Scale bar = 5 μ m. The images were taken for aggregated nanoparticles since confocal microscopes have limited resolution for clearly imaging a single nanoparticle. (H) Quantitative analysis of oxygen generated by ILTNP

incubation under hypoxia (1% O₂), $n = 7$. (I) Cell uptake of ILTONP by C2C12 cells (left), HUVECs (center), and THP-1 derived macrophages (right) after 2 h of treatment under hypoxia (1% O₂). Colocalization (yellow) of the ILTONP within cells is shown in yellow and highlighted by white arrows. Scale bars represent 50 μm for upper images and 20 μm for the expanded field of views (lower). (J) Quantification of internalization efficiency of ONP by three types of cells ($n = 7$). * $p < 0.05$, ** $p < 0.01$, *** $p < 0.001$, **** $p < 0.0001$.

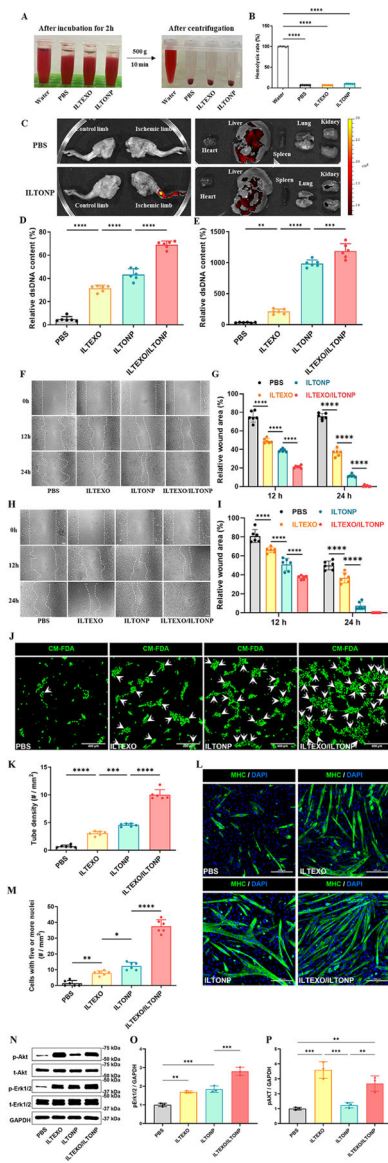


Figure 3. Characterization of ILTEXO and ILTONP in terms of hemocompatibility, ischemic limb-targeting ability, and biodistribution; and evaluation of the effect of ILTEXO and ILTONP on survival, migration, and morphogenesis of endothelial cells and myoblasts under high glucose and hypoxic conditions. (A) Appearance of bovine blood after incubation with ILTEXO or ILTONP for 2 h at 37 °C (left) and after centrifugation at 500g for 10 min (right). (B) The absorbance of hemoglobin (540 nm) released from broken red blood cells after 2 h of incubation and centrifugation ($n = 6$). (C) IVIS images of hindlimbs and major organs harvested 2 days after the IV injection of PBS or ILTONP. (D, E) dsDNA content of HUVECs (D) and C2C12 cells (E) after 5 days of incubation with PBS, ILTEXO, ILTONP, or ILTEXO/ILTONP under high glucose and hypoxic conditions ($n = 6$). (F) Migration of HUVECs incubated with PBS, ILTEXO, ILTONP, or ILTEXO/ILTONP under high glucose and hypoxic (1% O₂) conditions. Scale bar = 200 μ m. (G) Quantification of relative wound

areas after HUVECs cultured with different treatments under high glucose and hypoxic (1% O₂) conditions ($n = 6$). (H, I) Migration of C2C12 cells (H, scale bar = 200 μm) and relative wound areas (I, $n = 6$) after incubated with PBS, ILTEXO, ILTONP, or ILTEXO/ILTONP under high glucose and hypoxic (1% O₂) conditions. (J) Tube formation of HUVECs after 20 h incubation with PBS, ILTEXO, ILTONP, or ILTEXO/ILTONP under high glucose and hypoxic (1% O₂) conditions. Scale bar = 100 μm . (K) Quantification of tube density formed by HUVECs incubated with different treatments under high glucose and hypoxic (1% O₂) conditions ($n = 6$). (L) Myotube formation of C2C12 cells after 5 days of incubation with PBS, ILTEXO, ILTONP, or ILTEXO/ILTONP under high glucose and hypoxic (1% O₂) conditions. Scale bar = 200 μm . (M) Quantification of myotubes with five or more nuclei ($n = 6$). (N) Western blotting of phosphorylated Erk1/2 (p-Erk1/2) and phosphorylated Akt (p-Akt) in C2C12 cells cultured with PBS, ILTEXO, ILTONP, or ILTEXO/ILTONP under high glucose and hypoxic (1% O₂) conditions for 24 h. t-Erk1/2 and t-Akt were employed as internal references. (O, P) Quantification of p-Erk1/2 (O) and p-Akt (P). Expressions that are normalized to glyceraldehyde-3-phosphate dehydrogenase (GAPDH), $n = 3$. * $p < 0.05$, ** $p < 0.01$, *** $p < 0.001$, **** $p < 0.0001$.

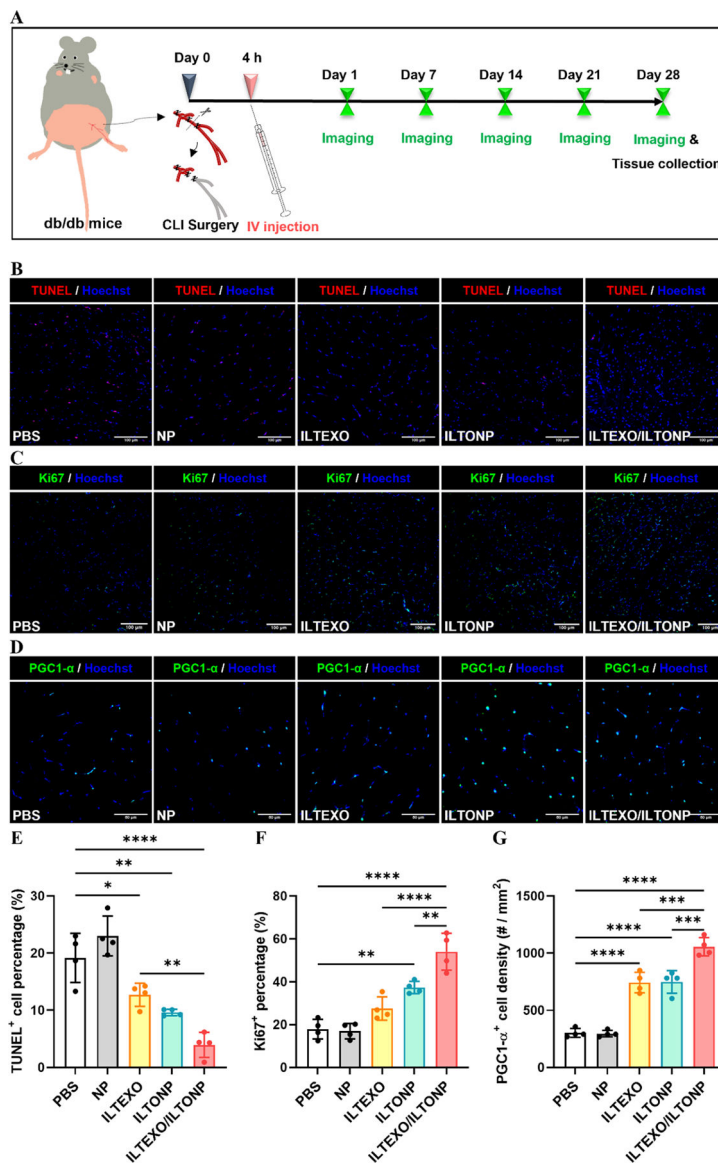


Figure 4. Co-delivery of ILTEXO and ILTONP promoted cell survival, proliferation, and mitochondrial metabolism in a diabetic CLI model. (A) CLI surgery and timeline for in vivo evaluation after IV injection of ILTEXO and ILTONP. (B) TUNEL staining of ischemic limbs harvested 4 weeks after CLI surgery. Scale bar = 100 μm . (C) Proliferation-associated protein Ki67 staining of ischemic limbs 4 weeks after IV injection. Scale bar = 100 μm . (D) PGC1- α staining of ischemic limbs 4 weeks after treatment. Scale bar = 50 μm . (E–G) Quantification of TUNEL⁺ apoptotic cells (E), Ki67⁺ proliferating cells (F), and PGC1- α ⁺ cells (G) in the ischemic limbs 4 weeks after treatment ($n = 4$). All nuclei were stained with Hoechst 33342. * $p < 0.05$, ** $p < 0.01$, *** $p < 0.001$, **** $p < 0.0001$.

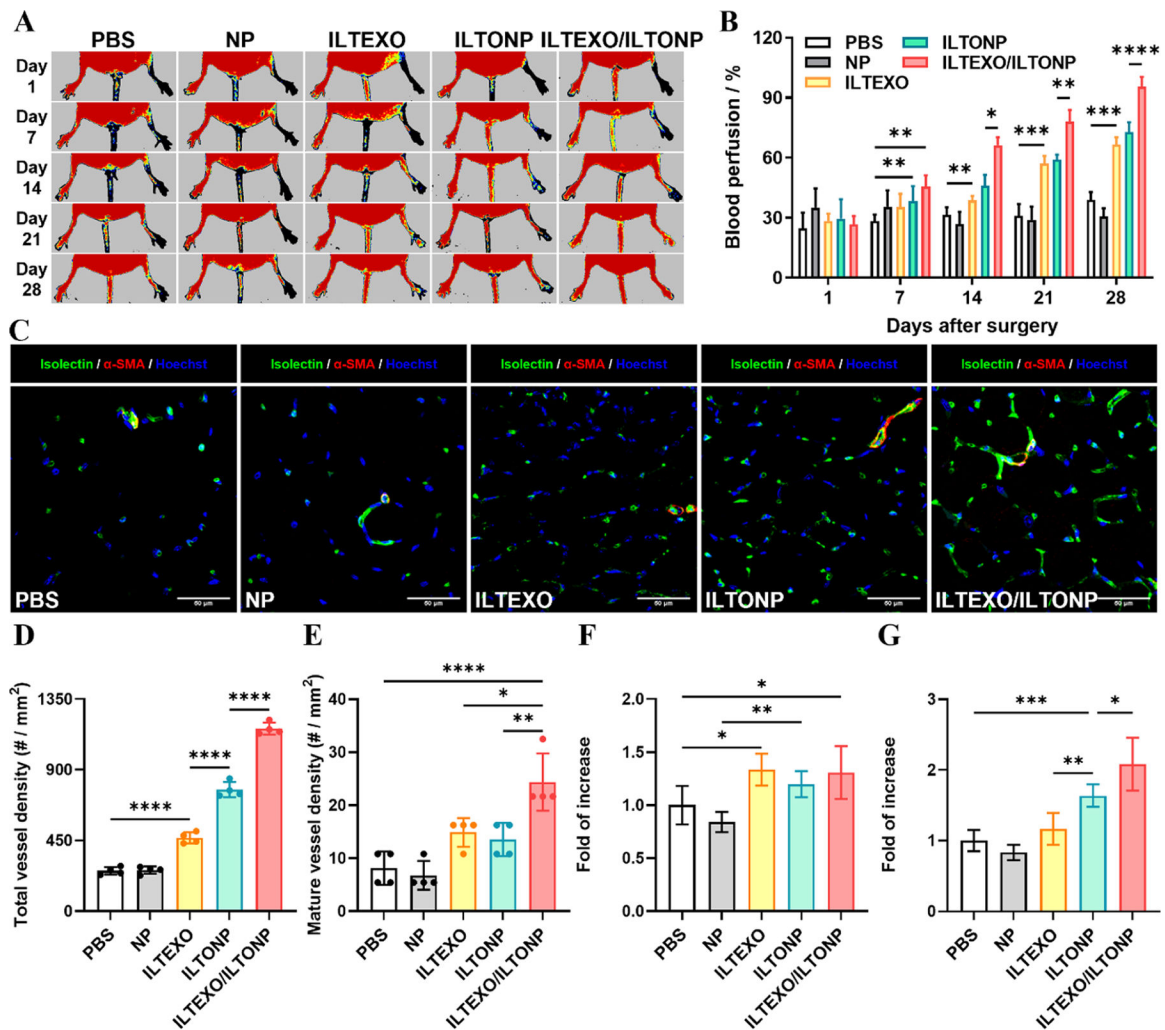


Figure 5.

ILTEXO and ILTONP stimulated tissue angiogenesis in a diabetic CLI model. (A) Laser Doppler perfusion images of diabetic mice after CLI surgery and receiving various administrations. (B) Relative blood perfusion of ischemic limbs normalized to the contralateral hindlimbs after different treatments ($n = 6$). (C) Immunohistochemical staining of isolectin (green) and α -SMA (red) in the ischemic limbs 28 days after treatment. Nuclei were stained with Hoechst 33342. Scale bar = 50 μ m. (D, E) Quantification of total vessel density (isolectin⁺ vessels, D) and mature vessel density (isolectin⁺/ α -SMA⁺ vessels, E). $n = 4$ for D and E. (F, G) Gene expression of Vegfa (F) and Fgf2 (G) in ischemic limbs 4 weeks after treatment ($n = 6$). * $p < 0.05$, ** $p < 0.01$, *** $p < 0.001$, **** $p < 0.0001$.

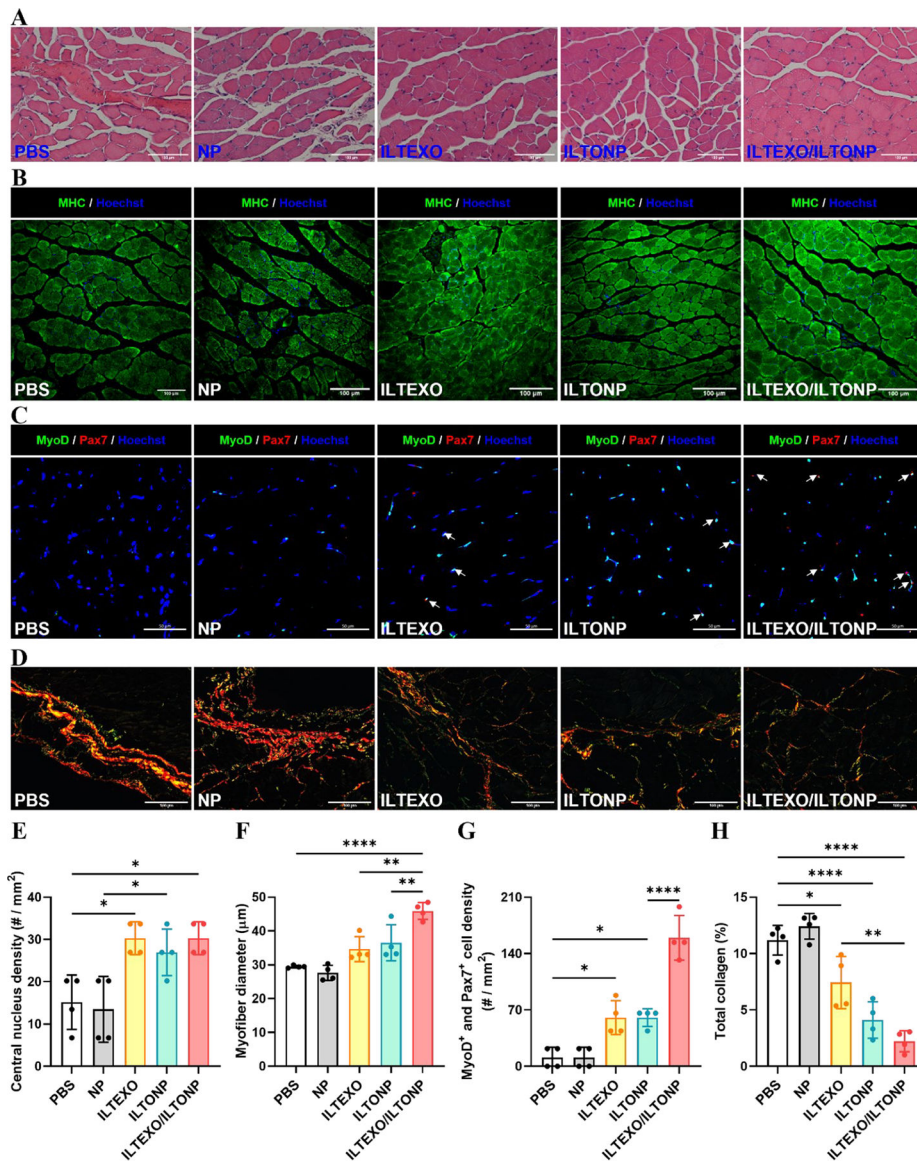


Figure 6. ILTEXO and ILTONP promoted skeletal muscle regeneration in a diabetic CLI model. (A) H&E staining for ischemic limbs 4 weeks after different treatments. Scale bar = 100 μm . (B) Immunohistochemical staining of MHC in the ischemic limbs 28 days after treatments. Nuclei were stained with Hoechst 33342. Scale bar = 100 μm . (C) Immunohistochemical staining of MyoD and Pax-7 in the ischemic limbs 28 days after treatments. Nuclei were stained with Hoechst 33342. Scale bar = 50 μm . (D) Picosirius red staining of collagen in the ischemic limbs 28 days after CLI surgery and receiving various administrations. Scale bar = 100 μm . (E–H) Quantification of central nucleus density (E), myofiber diameter (F), MyoD⁺/Pax-7⁺ cell density (G), and total collagen content (H) in the ischemic limbs 28 days after treatment ($n = 4$). * $p < 0.05$, ** $p < 0.01$, *** $p < 0.001$, **** $p < 0.0001$.

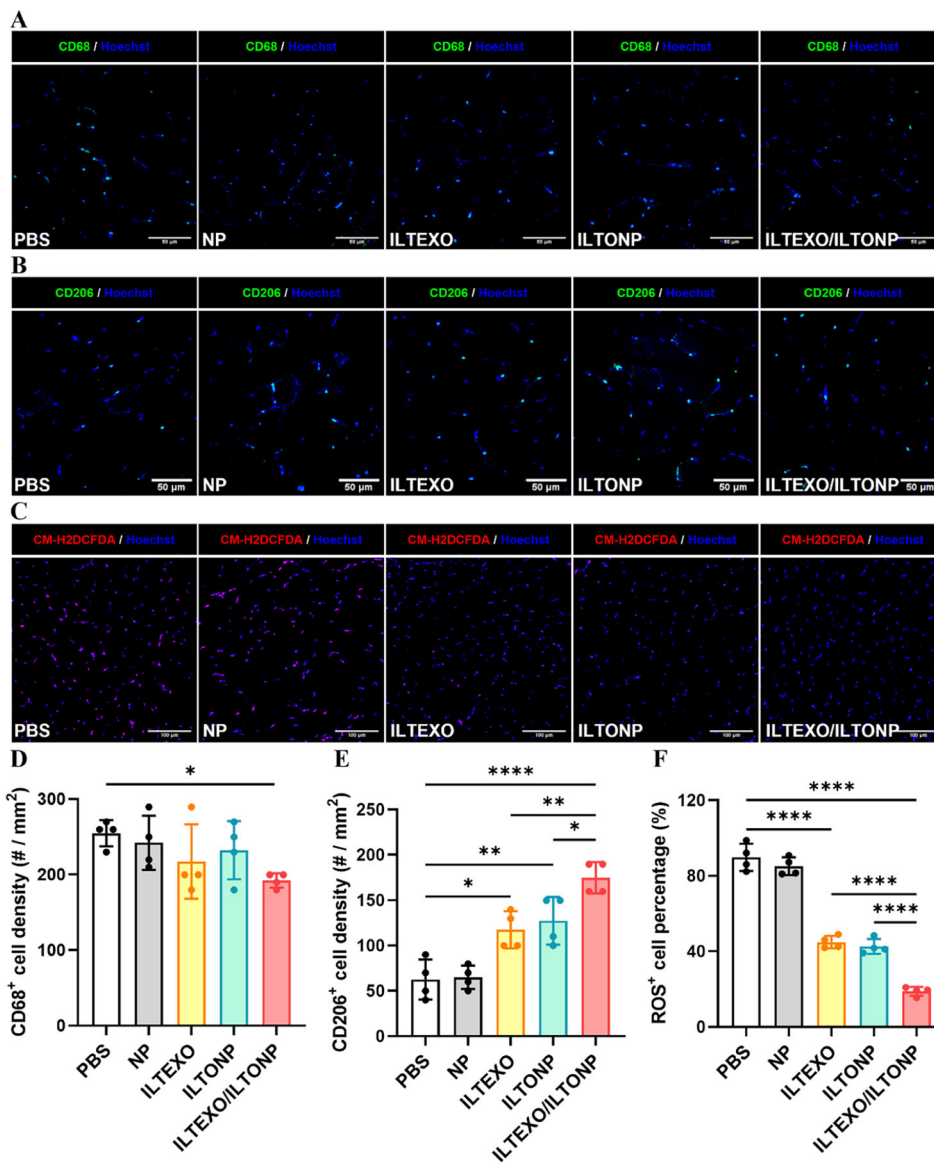


Figure 7. ILTEXO and ILTONP alleviated inflammation and oxidative stress in a diabetic CLI model. (A, B) Immunohistochemical staining of CD68 (A) and CD206 (B) in the ischemic limbs 28 days after different treatments. Scale bar = 50 μ m. (C) CM-H2DCFDA staining conducted in the ischemic limbs 28 days after various administrations. Scale bar = 100 μ m. (D–F) Quantification of CD68⁺ cell density (D), CD206⁺ cell density (E), and CM-H2DCFDA⁺ cell percentage (F) in the ischemic limbs 28 days after treatments. *n* = 4 for D–F. All nuclei were stained with Hoechst 33342 (blue). **p* < 0.05, ***p* < 0.01, ****p* < 0.001, *****p* < 0.0001.

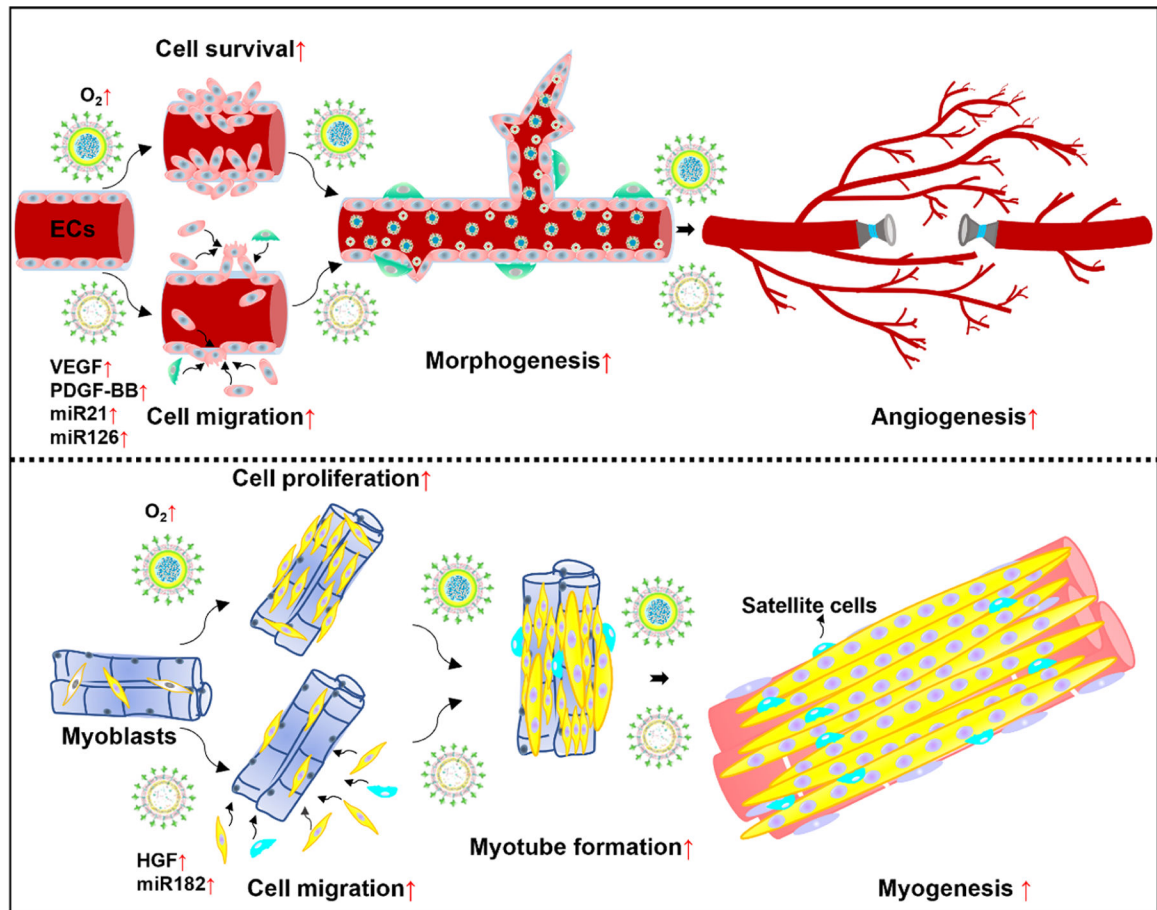


Figure 8. Mechanisms of synergistic effects of ILTEXO and ILTONP in promoting angiogenesis and myogenesis. The exosomes recruit endothelial and skeletal muscle cells. The released oxygen promotes survival of the recruited cells and those existing in the diabetic ischemic limbs before vascularization was established. The exosomes stimulated the morphogenesis of these cells.